

# **Localization of Excitatory and Inhibitory Neurotransmitter Receptors in an Identified Motoneuron of the Drosophila Flight System**

Dissertation zur Erlangung des akademisches Grades des  
Doktors der Naturwissenschaften (Dr. rer. Nat.)

Eingereicht im Fachbereich Biologie, Chemie, Pharmazie  
der Freien Universität Berlin

vorgelegt von

Claudia Kühn

aus Leipzig

Juni 2012

Die vorliegende Arbeit wurde unter der Leitung von Prof. Dr. Hans-Joachim Pflüger und Prof. Dr. Carsten Duch im Institut für Neurobiologie der Freien Universität Berlin, sowie der School of Life Science der Arizona State University angefertigt.

1. Gutachter: Prof. Dr. Hans-Joachim Pflüger
2. Gutachter: Prof. Dr. Carsten Duch

Disputation am 24. Juli 2012

*“To know the brain ... is equivalent to ascertaining the material course of thought and will, to discovering the intimate history of life in its perpetual duel with external forces.”*

*Santiago Ramón y Cajal*

*— Recollections of My Life, 1937 —*

## Acknowledgements

I would like to thank Dr. Carsten Duch and Dr. Hans-Joachim Pflueger for their support over the course of the three years of my PhD and beyond. I want to especially thank Dr. Duch for introducing me to the “Wild West”, accepting me in his new lab, and his support even when funding was limited. I also want to thank all other members of the Duch lab in Tempe: Jana Boerner, Erin McKiernan, Svea Hohensee. They enriched my life made my time there unforgettable. Special thanks go to Sandra Berger, who introduced me to MATLAB, which made my life a lot easier. Stevie Ryglewski, unfortunately, I only got to know her when I was already leaving. Nevertheless, our conversations in the dark room made a lasting and much appreciated impression. Many, many thanks to Fernando Vonhoff, a true friend, who’s supporting words, honesty, helpful attitude, and easy going nature helped me immeasurably through the harder times during my PhD and beyond. Many thanks also to scientists outside our lab, Julie Mustard and Irina Sinakevitch, who taught me many useful techniques and skills. I also want to thank Brendon Mott for the many fruitful discussions we had, and his much appreciated help during the editing phase of my thesis. Furthermore, I want to thank him for always believing in me, his kind support and love. I could not have done it without him. I also want to thank his family for their unconditional support, and for providing me a home in Tucson. Besonderer Dank gilt meinen Eltern, die immer ein offenes Ohr für mich haben und ohne deren Unterstützung in allen Lebenslagen die Erstellung dieser Arbeit nicht möglich gewesen wäre.

# CONTENTS

<b>1</b>	<b>Introduction.....</b>	<b>6</b>
1.1	Goals of this thesis.....	12
<b>2</b>	<b>Material and Methods .....</b>	<b>14</b>
2.1	Animals.....	14
2.2	Dissection.....	15
2.3	Intracellular Staining .....	15
2.4	Immunocytochemistry .....	16
2.5	Western Blot.....	18
2.6	Image Acquisition.....	19
2.7	Geometric Reconstructions.....	19
<b>3</b>	<b>Results.....</b>	<b>20</b>
3.1	Localization of Voltage Gated Sodium Channels in the Ventral Nerve Cord and MN5 .....	20
3.1.1	Documentation of Sodium Channel Immunocytochemistry Along the MN5 Neurite and Axon.....	21
3.1.2	Estimating The Spike Initiation Zone in MN5.....	23
3.2	Distribution Patterns of Putative Cholinergic and GABAergic Input Synapses on the MN5 Dendritic Tree .....	26
3.2.1	Localization of Putative Cholinergic Input Synapses on MN5 Dendrites .....	26
3.2.2	Localization of Putative GABAergic Input Synapses on MN5 Dendrites .....	34
3.2.3	Comparison Between nAChR and Rdl Distribution Patterns .....	42
3.3	Developmental Changes of Native $D\alpha 7$ nACh Receptor and Rdl Receptor Expression Pattern in the <i>Drosophila</i> Rentral Nerve Cord.....	42
3.3.1	$D\alpha 7$ Expression Patterns During Pupal Development of <i>Drosophila melanogaster</i> .....	43
3.3.2	Rdl Expression Patterns During Pupal Development of <i>Drosophila melanogaster</i> .....	45
3.3.3	Development of the MN5 dendritic Tree .....	47

---

<b>4</b>	<b>Discussion.....</b>	<b>48</b>
4.1	Estimating the Location of the Spike Initiating Zone in MN5.....	48
4.2	Spatial Separation of Putative Cholinergic and GABAergic Synapses to Different Dendritic Regions.....	50
4.3	Critical Analysis of the Method Used for Mapping Putative Synaptic Inputs to MN5 Dendrites.....	54
4.4	Nicotinic ACh and GABA <sub>A</sub> Receptor Expression Patterns During <i>Drosophila</i> Pupal Development.....	56
<b>5</b>	<b>Abstract .....</b>	<b>59</b>
<b>6</b>	<b>Zusammenfassung.....</b>	<b>60</b>
<b>7</b>	<b>References .....</b>	<b>62</b>

# 1 INTRODUCTION

The nervous system, with its millions of cells working in concert, is the key difference between plants and animals. It ensures survival by enabling the animal to pursue the four F's, fighting, feeding, fleeing, and reproduction. Although these principals have been known for centuries, how the nervous system facilitates particular tasks, or computations, and how these are implemented in neuronal networks to generate behavior, is one of the central questions in neuroscience (London & Haeusser, 2005). In 1897, Ramon y Cajal's neuron doctrine first described nerve cells as the functional unit of the nervous system. He described them as polarized cells, which receive signals at their root-like dendrites and transmit them through their axonal process. Modulation of information was thought to happen only at neuronal interconnection points, the synaptic switches (reviewed in: Bullock *et al.*, 2005). Building on a century of technological advancements in the fields of microscopy, electrophysiology, molecular biology and genetics, neurons have now been characterized as far more differentiated and complex units than Cajal originally anticipated (Bullock *et al.*, 2005). For instance, we now know that signals are not only modulated at interneuronal connections points, and the flow of information is not always unidirectional. Furthermore, axons and dendrites can now be distinguished according to the polarity of microtubule bundles (Bernhardt & Matus, 1984; Clark *et al.*, 1997), using molecular markers like kinesin for axons and nod for dendrites. Recent findings even suggest that dendrites release neurotransmitters (reviewed by: Urban & Castro 2010), a feature formerly only known to axon terminals.

Despite the wealth of new information about the nervous system that has been gathered over the past decades, the principle role of dendrites as the main input receiving structure in neurons remains, and they are still recognized as having a key role in facilitating interneuron communication and information flow in neuronal circuits. Dendrites were first described by Camillo Golgi in 1873. To unravel their role as primary substrate for neuronal information processing, their biophysical mechanisms have been under continuous investigation for the last 50 years (reviewed in: London & Haeusser, 2005; Koch and Segev, 2000; Haeusser & Mel, 2003). Rall's linear cable theory of dendrites in 1962 was a ground breaking attempt to examine the role of dendrites as computational units. By borrowing from contemporary knowledge about signal propagation in underground telegraph cables, these early computational models demonstrated that

dendritic morphology is a key factor in shaping local synaptic responses (Rall 1967, Rinzel & Rall 1974). It is therefore not surprising that shape and sizes of dendritic arbors are manifold (Ramon-Moliner, 1968; Johnston *et al.*, 1996). Since Rall's cable theory of dendrites, numerous studies have investigated the relationship of morphology and function. They found that specific parameters of the dendritic tree, like length, diameter, and branching complexity greatly affect integration of synaptic input and consequently influence the dynamics of action potential firing (e.g. Mainen & Sejnowski, 1996; Cuntz *et al.*, 2007; London & Häusser, 2005; Vetter *et al.*, 2001; Häusser *et al.*, 2000; Connors & Regehr 1996). Ultimately, these morphometric parameters enhance the neuron's computational power by introducing non-linear interactions between synapses and sub-compartments of the cell (Häusser & Mel, 2003). Furthermore, the dendritic arbor has to ensure the proper coverage of an area enclosing all required input-sites to ensure proper neuronal function and behavior. In fact, several neurological disorders, like fragile X syndrome, Huntington disease, and Rett syndrome, have been associated with misregulation and abnormalities in dendrite morphology (Lee *et al.*, 2011; Armstrong *et al.*, 1995; Berman *et al.*, 2012).

This requirement, that dendritic arbors sometimes need to cover relatively large areas in order to receive all necessary input, results in some synapses being located at great distance from the site of action potential initiation. Consequently, the impact of different synapses would be highly variable. In passive dendritic trees, the initiation of action potentials depends on the efficacy of individual excitatory synaptic responses and their summation (London & Häusser, 2005). The influence of an excitatory postsynaptic potential (EPSP) in turn depends on the initial size and shape of the synaptic response, as well as the cable properties of the dendritic tree, as it spreads to the site of action potential generation (Gulledge *et al.*, 2005, London & Häusser, 2005). Dendritic tapering and minimal path length can compensate for signal attenuation in complex dendritic trees, rendering a "democratic" tree in which all inputs provide similar depolarization (Cuntz *et al.*, 2007). Additionally, Magee and Cook (2000) found that hippocampal CA1 pyramidal neurons compensate for distance-dependent attenuation by increasing excitatory postsynaptic potential (EPSP) amplitude via a progressive increase in synaptic conductance. Furthermore, Nicholson *et al.* (2006) report a distance-dependent difference in synapse number, and they propose this as a mechanism for counteracting voltage attenuation in dendrites of hippocampal CA1 pyramidal neurons.

Likewise, parallel processing and local computations greatly influence neuronal output. Building on his basic models, Rall *et al.* (1967) predicted that if two excitatory inputs are active together at short distance, the response to the stimulatory activation is smaller than the sum of the individual responses. This concept of spatial summation suggests that one possible function of complex dendritic trees is the spatial separation of synaptic inputs to enhance their summation at the site of action potential generation (Gulledge *et al.*, 2005; Redman & Walmsley, 1983; Markram *et al.*, 1997; Tamas *et al.*, 2002). In other cases, however, sublinear summation is advantageous; for instance, it is essential for coincidence detection in auditory neurons (Agmon-Snir *et al.*, 1998). Taken together, these studies indicate a strong correlation between form and function in dendritic trees. Multiple studies examining mental retardation, for instance, determined a direct relationship between either reduction in dendritic branch complexity or length, or changes in dendritic spines as a consistent feature and an index for major neuronal disruption (reviewed in: Kaufmann & Moser, 2000). Therefore, the geometry of neurons and the placement of synapses are critically important for single cell computation, normal brain function, and proper behavior.

Yet another aspect of neuronal computation is the interplay between excitatory and inhibitory synaptic inputs. Inhibition in the hippocampal formation, for instance, is regulated by inhibitory interneurons, which control both neuronal synchronization and the global level of activity (Esclapez *et al.*, 1997; Boullieret *et al.*, 2000; Cossart *et al.*, 2001; Dinocourt *et al.*, 2003; van Vliet *et al.*, 2004). Hypersynchronous network events, which are a common feature in all epilepsy syndromes, are thought to be caused by an increase in the excitation-inhibition ratio in the hippocampal area CA1 (Stief *et al.*, 2007). In the mammalian and insect nervous systems, fast synaptic inhibition is mediated primarily by  $\gamma$ -aminobutyric acid (GABA) acting on GABA<sub>A</sub>-type receptors (Burrow, 1996; Barnard *et al.*, 1998). The ability of GABA to inhibit action potentials is primarily due to its capability to diminish concurrent EPSPs by lowering the membrane potential below action potential threshold (Gulledge *et al.*, 2005; London & Haeusser, 2005). This phenomenon, called shunting inhibition, has several computational consequences. First, it is temporally precise, inhibiting action potential generation during only the few milliseconds that GABAergic conductance is active (Staley & Mody, 1992; Gulledge & Stuart, 2003a). Second, it is spatially restricted (Rall 1964). Therefore, when excitatory and inhibitory inputs are proximate to each other on dendritic branches, the inhibition can produce a highly nonlinear “shunting” of excitatory input (London & Haeusser, 2005;

Rall, 1967; Jack *et al.*, 1975; Koch *et al.*, 1990). Shunting inhibition can therefore provide effective inhibition to defined subregions of the dendritic tree (Gulledge *et al.*, 2005; Liu, 2004). Consequently, the relative position of inhibitory synapses to excitatory synapses determines whether they counteract a specific set of neighboring excitatory synapses, or act on a larger set of excitatory synapses when they are located between excitatory input and the site of action potential initiation (London & Häusser, 2005). The presence of active dendritic conductance through various ion channels further enhances dendritic computation (Gulledge *et al.*, 2005). These ion channels can enhance the ability of single excitatory inputs to cause action potentials, independent of their synaptic location on a dendritic tree (Miles, 1990). Furthermore, distal EPSPs can be amplified with the combination of appropriately timed back-propagating action potentials (Stuart & Häusser, 2001; Mehta, 2004; Nicholson *et al.*, 2006).

In order to implement the computational processes described above, it is essential for the right synapse to be addressed to the right dendrite. Pyramidal neurons are one of the best studied classes of neurons. Excitatory input facilitated through AMPA receptors ( $\alpha$ -amino-3-hydroxy-5-methyl-4-isoxazolepropionic acid receptors) in pyramidal cells has been shown to increase at distal dendrites in a distance-dependent manner (Magee & Cook, 2000; Andrasfalvy & Magee, 2001). GABAergic synapses in this type of vertebrate neuron are directed to the soma, distal dendritic regions, and the axon initial segment (Somogyi *et al.*, 1998; Di Cristo *et al.*, 2004). Di Cristo *et al.* (2004) further suggest that targeting mechanisms for these GABAergic synapses are largely genetically pre-determined and independent of experience. Similarly, Meseke *et al.* (2009) have shown that invertebrate GABAergic synapses in *Manduca sexta* localize at more distal dendrites in the adult motor neuron MN5. Interestingly, the larval GABAergic synapse distribution in the same motor neuron (MN5) appeared to be random. It was suggested that this change in distribution accompanied a change in function from a slow larval crawling to a fast adult flight motor neuron (Meseke *et al.*, 2009). Furthermore, Meseke *et al.* (2009) propose that, based on a homogenous neuropil structure with respect to GABAergic synapses, the specific distribution patterns are the consequence of sub-dendritic targeting and not due to a high density of GABAergic neurons in these areas. Taken together, these findings suggest genetically pre-determined distribution patterns of synapses to subregions of complex dendritic trees during neuronal circuit formation. Distinct molecular compositions within distinct compartments of dendrites and axons have been recently reported as possible mechanisms facilitating the process of compartment-specific

localization (reviewed in: Horton & Ehler, 2003; Katsuki *et al.*, 2011). However, the complexity of cortical networks in the mammalian brain makes the assessment of behavioral consequences of pyramidal cell computation resulting from sub-dendritic synapse and ion channel distribution difficult (Katz *et al.*, 2009). Analysis of dendritic computation is most powerful when the role of the neuron is understood and applied modifications can be tested in behavioral experiments. Invertebrate nervous systems, with their conserved physiology, morphology and function from animal to animal, have been crucial and fruitful model systems in the attempt to unravel complex molecular, genetic, and neuronal relationships.

Holometabolous insects like *Drosophila melanogaster* are well suited for the investigation of the structural and functional development of dendrites (Weeks & Levine, 1995; Grueber *et al.*, 2003). Furthermore, *Drosophila* offers a powerful genetic tool-kit. The UAS-GAL4 system, in combination with enhancer trap lines, allows the targeted expression of various genes in sub-populations of cells, which can be visualized by the expression of reporter genes like the green fluorescent protein (GFP; Brand & Perrimon, 1993; Bellen *et al.*, 1989). These tools combined with short generation times and high fecundity, allowed fast assessment and provided fundamental insight into molecular mechanisms underlying dendritic development and morphology over the past decades (Luo, 2000; Moore *et al.*, 2002; Jefferis *et al.*, 2001; Komiyama & Luo, 2007). The giant fiber system, which controls escape behavior in *Drosophila*, has been proven to be a valuable system to link behavior to cellular function (Engel & Wu, 1996, 1998; King & Wyman, 1980). Further, the morphology and physiology of the flight motor neuron MN5, which is part of the escape circuit, has been investigated in great detail (Consoulas *et al.*, 2002; Duch *et al.*, 2008; Ryglewski and Duch, 2009; Vonhoff and Duch, 2010), and its firing patterns during flight and courtship behavior are well described (Levine & Wyman, 1973; Harcombe & Wyman, 1977; Ewing, 1977).

Together with four other motor neurons (MN1-4), MN5 innervates the dorsal longitudinal flight muscle (DLM; Figure 1). The DLM is an asynchronous muscle responsible for wing depression during *Drosophila* flight. It consists of six muscle fibers (Figure 1B). Fibers one to four are innervated ipsilaterally by MN1-4, and fibers five and six are innervated contralaterally by MN5 (Ikeda & Koenig, 1988; Duch *et al.*, 2000). MN5's large cell body lays on the dorsal surface of the mesothoracic ganglion in the ventral nerve cord (VNC) in *Drosophila*, making it easily accessible for intracellular

staining and recording (Figure 1A). All five flight motor neurons are born embryonically. MN1-4 innervate the DLM precursor muscle in the larva, whereas MN5 remains dormant until pupation (Consoulas *et al.*, 2002), when it obtains its behavioral function and physiological properties (Consoulas *et al.*, 2000). Simultaneous recordings from MN1-5 during restrained flight revealed that MN1-5 fire tonically at similar frequencies but never in synchrony (Koenig & Ikeda, 1980a, b; Levine & Wyman, 1973; Harcombe & Wyman, 1977). Furthermore, tonic firing rates of these motor neurons change in response to different power demands (Gordon & Dickinson, 2006). Harcombe and Wyman (1977) hypothesized that common excitatory drive to MN1-5 is translated into tonic, slowly adjustable firing frequencies, and that inhibitory network connections prohibit simultaneous MN1-5 firing. Considering, the genetic tool-kit available for *Drosophila*, the relatively small size of the VNC that enables whole mount imaging, and the known characteristics of MN5, make it an ideal model neuron to unravel the complex interplay between synaptic and dendritic computation as described above.

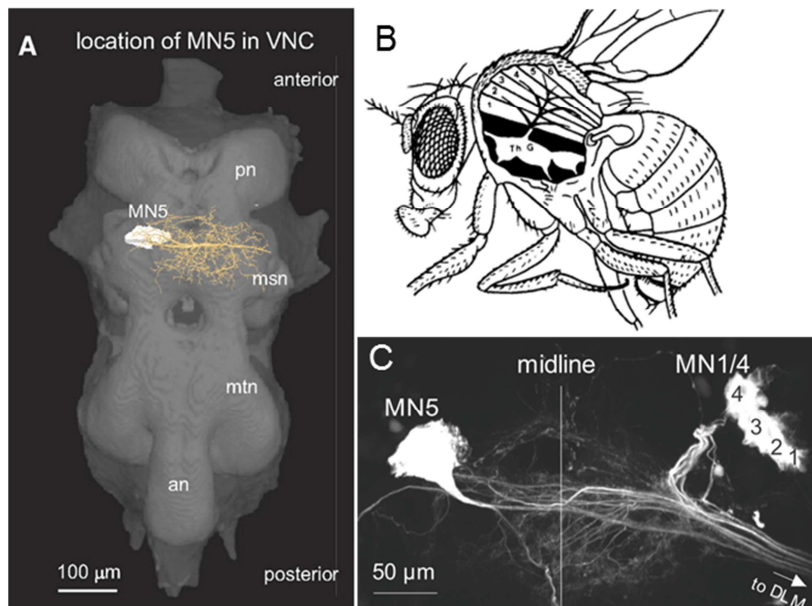


Figure 1: *Motor neuron MN5 relative position within the Drosophila ventral nerve cord (VNC) and to the dorsal longitudinal flight muscle (DLM).*

- A) Schematic drawing of dorsal view of the adult *Drosophila* ventral nerve cord (VNC; pn, prothoracic neuromere; msn, mesothoracic neuromere; mtn, metathoracic neuromere; an, abdominal neuromere). MN5 is located in the msn close to the dorsal surface, with its cell body contralateral to the axonal projection. The dendrites cover a large area of the msn. Figure from: Ryglewski & Duch, 2009.
- B) Diagrammatic representation of the DLM of *Drosophila melanogaster*. The six single muscle fibers are numbered from the most anterior insertion. The posterior dorsal mesothoracic nerve (PDMN) from the thoracic ganglion (Th G) innervates these

muscle fibers. The median branch is shown on the surface of the muscle. Figure from: Ikeda *et al.*, 1980.

- C) Location and overall dendritic structure of the flight motoneurons MN1-5 as revealed by selective retrograde staining from the DLM flight muscle. Figure from: Duch *et al.*, 2008.

## 1.1 GOALS OF THIS THESIS

In this study I aimed to provide a foundation for the analysis of the relationship between form and function in complex dendritic trees. Using the model neuron MN5 in *Drosophila*, for which morphology and behavioral patterns have been well characterized, I asked whether there are specific rules for sub-cellular targeting of excitatory and inhibitory input synapses. The balance and relative location between excitatory and inhibitory input on dendritic branches and whole dendritic trees is thought to have a critical effect on signal integration and dendritic computation (e.g., London & Häusser, 2005; Di Cristo *et al.*, 2004; Liu, 2004; Cline, 2005). In the case of MN5, it has been hypothesized that the correct time point for MN5 firing might be controlled by inhibitory input (Harcombe & Wyman, 1977). The correctly timed firing of MN5 in concert with MN1-4 is necessary to ensure adequate contraction of the DLM (Harcombe & Wyman, 1977, Ikeda & Koenig, 1980a, b; Levine & Wyman, 1973). By generating synaptic distribution maps and analyzing the localization of excitatory and inhibitory input, this study is meant to aid our understanding of the developmental, physiochemical, and computational mechanisms that underlie these specific firing patterns observed in *Drosophila*. In the insect VNC, nicotinic acetyl choline receptors (nAChRs) mediate fast excitatory input (Leech & Satelle, 1993), and GABA<sub>A</sub> receptors are predominantly used for fast inhibitory input (Raghu *et al.*, 2007). The *Drosophila* genome contains 10 nAChR subunits, of which the Dα7 subunit is homologous to vertebrate α7 receptors (Grauso *et al.*, 2002). Dα7 forms homomeric pentamers, which are highly permeable for calcium, and it is the predominant nAChR of all neurons in the *Drosophila* escape circuit, including MN5 (Fayyazuddin *et al.*, 2006). GABA<sub>A</sub>-Rs are GABA-gated chloride channels encoded by at least three genes in *Drosophila*, of which Rdl (resistance to dieldrin) is the best characterized. It is abundantly expressed in the *Drosophila* brain (French-Constant *et al.*, 1990, 1993; Harrison *et al.*, 1996; Liu *et al.*, 2007; Agosto *et al.*, 2008), and it is localized on central neuron dendrites (Raghu *et al.*, 2007). To investigate the specific

distribution patterns of excitatory and inhibitory input, I used targeted expression of tagged GABA<sub>A</sub> receptors (Rdl) and nAChRs (Da7 subunit) under the control of motoneuron-specific GAL4 drivers, as well as immunocytochemistry. High resolution confocal laser scanning microscopy and co-localization analysis (Schmitt *et al.*, 2004; Evers *et al.*, 2005) were combined with MN5 intracellular staining to map distribution patterns for putative cholinergic and GABAergic synapses in the *Drosophila* non-layered neuropil (Boerner & Duch, 2010) onto three-dimensional surface reconstructions of MN5.

However, to evaluate the significance of certain synaptic distribution patterns it is vital to identify the location of the spike initiating zone (SIZ), where all input information is eventually measured against a threshold. MN5 action potential generation requires TTX sensitive, voltage-gated sodium channels (VGSC; Duch *et al.*, 2008; Ryglewski & Duch, 2009; Ryglewski *et al.*, 2012). Therefore, all parts of the MN5 neuron involved in active action potential propagation should exhibit high densities for VGSC in the membrane. To estimate the area of action potential initiation in MN5, I combined sodium channel immunocytochemistry with MN5 intracellular staining to trace sodium channel expression along the neuron. Further, I used these data to develop a method that enables estimation of the SIZ location in animals without sodium channel immunocytochemistry.

Numerous studies on dendritic development have shown that dendritic morphology is regulated by various genetic factors (Montague & Friedlander, 1989; 1991; Spatkowski & Schilling, 2003; Gao & Bogert, 2003), guidance cues (Kim & Chiba, 2004; Landgraf & Thor, 2006), growth factors and hormones (Weeks & Levine, 1995; Cooke & Wooley, 2005), and neural activity (reviewed in Wong & Ghosh, 2002; Flavell & Greenberg, 2008). Studies in insects like *Manduca sexta* and *Drosophila* have shown that activity plays a crucial role in the structural development of dendritic trees. An increase in activity has been shown to promote dendritic growth in developing larvae and adult insects (Hartwig *et al.*, 2008; Duch *et al.*, 2008; Meseke *et al.*, 2009). Nicotinic AChRs are highly permeable for calcium (Oliveira *et al.*, 2010). Calcium changes, both locally (i.e., nAChRs and ion channels) and globally throughout the neuron (i.e., internal calcium stores), have been correlated to changes in gene expression via activity dependent regulators such as CREB or Crest (West *et al.*, 2002; Flavell & Greenberg, 2008; Redmond & Ghosh, 2005). However, the mechanisms that mediate dendritic growth in an activity dependent manner through development are poorly understood. Within the scope of this study, I investigated the native expression pattern of nAChRs and GABA<sub>A</sub>-Rs in the VNC throughout pupal

development of *Drosophila* using immunocytochemistry against Da7-subunit and Rdl. Together with MN5 intracellular stainings in critical pupal stages, I discuss a possible role of these receptors during early dendrite formation and synaptogenesis.

This study is meant to provide a framework that will allow us to unravel the timing of excitatory and inhibitory synapse placement during development, and this should help us elucidate the factors facilitating dendritic growth in complex dendritic trees. Furthermore, this study should add to our understanding of the interdependent suite of morphological and computational characteristics that enable the motoneuron 5 to elicit specific and correctly timed firing patterns, which are necessary for proper escape, flight and courtship behaviors.

## 2 MATERIAL AND METHODS

### 2.1 ANIMALS

*Drosophila melanogaster* strains were kept in 68 ml vials on standard corn meal medium at 25°C (12/12 light/dark cycle) and 50-60% humidity. For experiments, female adult flies (F1 generation) were used one to three days after eclosion. Staging of pupae was conducted according to Brainbridge & Bownes (1981). The GAL4-UAS system (Brand and Perrimon, 1993; Duffy, 2002) was utilized to express genes of interest, cloned to UAS elements, under the control of two recombinant motoneuron driver lines C380-GAL4, and P103.3-GAL4, respectively (Sanyal *et al.*, 2003; 2009; Consoulas *et al.*, 2002). Homozygous virgins from these two GAL4 driver lines were crossed with male flies that were homozygous for the various UAS-constructs. Unwanted expression of GAL4 in interneurons was prevented by using Cha-GAL80 (choline-acetyl transferase promotor driven GAL80), which has been shown to suppress GAL4 activity in all cholinergic neurons (Aberle *et al.*, 2002). The recombinant lines C380-GAL4; Cha-GAL80, (with and without UAS-mCD8-GFP construct) were received from Dr. S. Sanyal (Emory University, Atlanta, GA). Transgenic flies carrying the UAS-Da7-GFP construct to express GFP-tagged Da7 subunits of the nicotinic acetylcholine receptor (Raghu *et al.*, 2009) were obtained from Dr. S. Sigrist

(Free University of Berlin, Germany). Transgenic flies carrying the UAS-HA-tagged Rdl-GABA-A receptor subunit (Raghu *et al.*, 2007) were obtained from Dr. A. Prokop (University of Manchester, U.K.).

## 2.2 DISSECTION

Animals were anesthetized by chilling them on ice in an empty vial for 10-15 min. First, the wings and legs were cut off to enable proper placement dorsal side up on a sylgard-coated (Dow Corning Co., Midland, MI) petri dish. The animals were then covered with standard saline (Jan & Jan, 1976). The thorax was opened by making an incision along the dorsal midline between the two dorsal flight muscles. Minuten-pins were pierced gently through the muscle and cuticle to hold the thorax open. After cutting off the head, all dorsally laying organs were removed gently to expose the ventral nervous system.

## 2.3 INTRACELLULAR STAINING

MN5 intracellular staining was performed as previously described by Duch *et al.* 2008. First, the petri dish was mounted onto the fluorescent microscope. Prior to the labeling procedure application of 1% collagenase locally over the MN5 cell body for 10 seconds ensured easy penetration with the dye-filled electrode. The preparation was washed thoroughly with saline to stop the digestive process. For intracellular labeling, a thin walled glass microelectrode (75-95 M $\Omega$  tip resistance) was filled with a mixture of 7% neurobiotin (Linaris GmbH, Wertheim-Bettingen, Germany) and Rhodamin-Dextran (Invitrogen, Carlsbad, CA, U.S.) in 2 M potassium acetate. To avoid dye dilution, an air bubble was left between the dye filled tip and the potassium acetate in the shaft. After penetrating the MN5 cell body, the dye was injected iontophoretically by a constant depolarizing current of 0.5 nA for 10-12 minutes. After removal of the electrode, the saline was immediately replaced by the appropriate fixative.

## 2.4 IMMUNOCYTOCHEMISTRY

Double labeling for tagged receptors ( $D\alpha 7$ -nAChRs and Rdl-GABA-ARs), sodium channel (SP19), and MN5 intracellular staining was conducted by combining immunohistochemistry protocols for SP19, GFP or HA (see below) with intracellular neurobiotin staining protocol (see above). The lack of cross-reactivity of the secondary antibodies in double- and triple-labeling experiments was consistently checked (data not shown).

### *Immunocytochemistry for GFP-tagged $D\alpha 7$ subunits of the nicotinic acetylcholine receptor*

After intracellular staining of the MN5, the tissue was fixed for 30 minutes with 4% paraformaldehyde in 0.1 M phosphate buffer solution (PBS). Samples were rinsed and washed over night in PBS (0.1 M) at 4°C. Following several washing steps (9 times for 20 minutes each) in PBS (0.1 M) with 0.5% TritonX (TX, Sigma) at room temperature, samples were incubated with primary anti-GFP antibody (Invitrogen, rabbit anti-GFP, A11122; 1:400) and mouse NC82 (Developmental Studies Hybridoma Bank; 1:100) in 0.1 M PBS TX 0.3% and 3% bovine albumin serum (BSA) for 24h at 4°C. The next day, samples were washed in 0.1 M PBS (6 times 30 minutes). Secondary antibodies against rabbit were conjugated with Cy2 (1:500), those against mouse were conjugated with Cy5 (1:500), and streptavidin was conjugated with Cy3 (1:750; Jackson Immuno Research). Incubation of secondary antibodies occurred over night at 4°C in PBS (0.1 M) and 2% normal goat serum (NGS). Then the samples were washed with 0.1 M PBS. Prior to mounting the samples in methyl salicylate, they were dehydrated in an ascending ethanol series (50%, 70%, 90%, 100%, diluent 0.1 M PBS, 15 minutes each), and incubated in a 1:1 100% ethanol-methyl salicylate mixture for 5 minutes.

### *Immunocytochemistry for the UAS-HA tagged Rdl GABA<sub>A</sub>-Rs*

As fixative a 4% paraformaldehyde in 0.1 M PBS solution was applied for 30 minutes. Prior to the application of primary antibodies the samples were washed with 1% TX in 0.1 M PBS for 1h at room temperature. Primary antibodies against HA (hemagglutinin; rat; 1:200) were incubated for 24h at 4°C in 1% TX PBS (0.1 M) and 2% NGS. After rinsing and washing the samples with PBS (0.1 M), secondary antibodies anti-rat conjugated with Cy5 and streptavidin conjugated with Cy3 were applied as described above. Samples were

mounted in methyl salicylate after dehydration via an ascending ethanol series (see above).

### *Immunocytochemistry for sodium channels*

For the labeling of sodium channels, the polyclonal antibody (Chemicon International, AB5210) against the purified peptide SP19 of the alpha subunit (amino acids 1500-1518) of rat type I VGSC (accession no. P04774) was used at the recommended dilution of 1:200. Specificity of the SP19 antibody for insect sodium channels was demonstrated in multiple studies (French *et al.*, 1993; Amat *et al.*, 1998; Boerner *et al.*, 2006). In addition, this study also confirmed the specificity by western blotting (see below). Prior to the incubation of primary antibodies, the samples were washed in 0.5% TX PBS (0.1 M) for 3h (9 times for 20 minutes each). Primary antibodies SP19 (rabbit; 1:200) and NC82 (mouse; 1:100) were applied in 0.3% TX PBS (0.1 M) and 2% BSA for 24h at 4°C. After rinsing and washing the samples with 0.1 M PBS, secondary antibodies against rabbit, mouse and streptavidin were applied as described above. Samples were mounted in methyl salicylate following the protocol described in detail above.

### *Immunocytochemistry for D $\alpha$ 7 nAChR*

Immunocytochemistry utilizing primary D $\alpha$ 7 nAChR antibody (kind gift of Dr. H. Bellen, BCM, Houston Texas) was used to document D $\alpha$ 7 nAChR expression patterns during pupal development of *Drosophila melanogaster*. Pupal preparations were treated in the same dish, under the same conditions, and images were acquired with the same settings using the larva preparation as a standard. Fayyazuddin *et al.* (2006) have shown D $\alpha$ 7 nAChR antibody specificity and absence of immunolabel in null mutants. Samples for immunocytochemistry were fixed in 4% paraformaldehyde and 0.1 M PBS for 15 minutes. Next, samples were rinsed and washed with 0.1 M PBS over-night at 4°C. This was followed by several washing steps (9 times 20 minutes each) with 0.5 % TX in PBS (0.1 M) at room temperature. The rat anti-D $\alpha$ 7 nAChR antibody (1:2000) was applied for 48h in 0.3% TX PBS (0.1 M) and 3% BSA at 4°C. Samples were then washed with PBS (0.1 M), incubated with anti-rat secondary antibodies and mounted, following the protocol described above.

### *Immunocytochemistry for Rdl GABA<sub>A</sub>-Rs*

For documentation of native Rdl GABA<sub>A</sub>-Rs expression during pupal development, primary rabbit anti-Rdl GABA<sub>A</sub> receptor antibody was used (kind gift of Dr. Naessel,

Stockholm, Sweden). Antibody specificity has been shown previously by Enell *et al.* (2007). Pupal preparations were treated in the same dish, under the same conditions, and images were acquired with the same settings. After animal dissection, the samples were fixed in 2% formalin and 1% sodium metabisulfite (SMB, Sigma) for 30 min at room temperature, and then washed and rinsed for 2h with 0.1 M PBS. As preparation for primary antibody application, samples were then treated with 0.5% TX PBS for 3h (9 times for 20 minutes). Primary rabbit anti-Rdl antibody was applied for 24h at 4°C in 0.3% TX PBS (0.1 M) and 2% NGS at a dilution of 1:10000. Samples were then washed with PBS (0.1 M), incubated with anti-rabbit secondary antibodies and mounted, following the protocol described above.

## 2.5 WESTERN BLOT

Specificity of the SP19 antibody for insect sodium channels has been previously shown by French *et al.* (1993), Amat *et al.* (1998), and Boerner *et al.* (2006). However, to confirm specificity in *Drosophila* nervous tissue, Western Blot analysis was conducted. *Drosophila* thorax preparations were collected on ice in 6x sample buffer with protease inhibitors. After dissection, the tissue was homogenized and heated for 5 minutes at 70°C. The samples (~ 5 thorax = 25 µl per lane) were loaded together with a molecular weight marker (Bio Rad Precision Plus Protein Kaleidoscope Standards no. 161-0375) on the gel. The stacking gel ran for 2h at 13-15 mA, and the 5% separating gel ran for 5h at 30-35 mA at 4°C. The transfer was conducted using wet conditions and ran for 2h at 0.45 A at 4°C. Ponceau staining was used to visualize the lanes before cutting the membrane. The membranes were then blocked with 10% nonfat milk in TBS (+Tween) for 1h at room temperature. Primary antibody rabbit SP19 (Chemicon; AB5210) was diluted 1:200 in 2% nonfat milk in TBS (Tris-buffered saline+Tween) and incubated over night at 4°C. Prior to secondary antibody application the samples were rinsed and washed (6 times 15 minutes) with 10% nonfat milk in TBS (+Tween). Peroxidase conjugated affinity purified anti-rabbit IgG (611-1322) was diluted 1:10000 in 2% nonfat milk in TBS (+Tween) and incubated for 2h at room temperature. Samples were rinsed and washed (3 times 15 minutes) with TBS (+Tween), last wash with TBS (no Tween). For image acquisition detection solution (Immobilon Western Chemiluminescent HRP Substrate, no. WBKLS0100) was applied for 3 minutes.

## 2.6 IMAGE ACQUISITION

All images were attained with a Leica SP2 confocal laser scanning microscope using a 40x oil-immersion objective (numerical aperture 1.2) at a resolution of 1024 x 1024 pixels and a z-step size of 0.3  $\mu\text{m}$  for high resolution scans, and 0.7  $\mu\text{m}$  for lower resolution overview scans. Maximum optical resolution for high resolution scans was 120 nm x 120 nm x 300 nm.

Cy2 was excited with an argon laser at 488 nm and detected between 500 and 530 nm. Cy3 was excited with a Krypton laser at 568 nm and detected between 575 and 620 nm, and Cy5 was excited with a helium neon laser at 633 nm and detected between 640 and 700 nm. Cy2 and Cy5 were excited and detected simultaneously, but Cy3 was scanned in sequential scan mode with excitation switching between each frame. At the moderate laser and detector intensities needed no bleed through between any of the three channels was observed. All images were saved as tiff stacks and further processed with AMIRA 4.1.1 (Mercury Systems), Adobe Photoshop, Adobe Illustrator. Images shown are either projection views, projecting all optical sections into one plane by using the maximum intensity criterion, or single slide pictures, just showing one optical section.

## 2.7 GEOMETRIC RECONSTRUCTIONS

Three-dimensional geometric reconstructions of the central arborizations of the identified *Drosophila* motoneuron, MN5, were conducted with custom plug-ins for Amira 4.1 (Mercury), which have been described in detail elsewhere (Schmitt *et al.*, 2004; Evers *et al.*, 2005; Meseke *et al.*, 2009). These deliver precise quantifications of midline and diameter of neuronal processes and create based on this information a triangulated surface. Each triangle is located perpendicular to the midline of the corresponding reconstructed segment (for details see Evers *et al.*, 2005). To quantify the distributions of the various immunolabels, voxels were only measured if they satisfied two criteria: They must be within a given distance from the reconstruction's calculated surface, and their intensity must exceed a designated threshold. In the case of nAChR distributions, a triangle on the reconstruction surface was counted positive when it was in close proximity to NC82 (300 nm) and D $\alpha$ 7-immunolabel (100 nm) (see details in Evers *et al.*,

2005; Meseke *et al.*, 2009). In the case of Rdl receptor and sodium channel distribution, a triangle was counted positive when it was in the same voxel (100 nm) as the immunolabel for Rdl or sodium channel, respectively. Quantitative morphometric data (Amira generated ASCII-tables) were imported into Microsoft Excel for further analysis. Briefly, amounts and densities were used to quantify the findings. Amounts were calculated by the summation of all positive triangles. Densities were calculated by the summation of positive triangles and relating this sum to the total number of triangles pertaining to a branch or certain distance measure. The result describes the density of positive triangles in that area in a percent value. Electron microscopy demonstrated that this procedure accounted for all synaptic terminals located in the thoracic motor neuropils of *Manduca*, but also produced approximately 20 percent false positive synapses if only one immunolabel was used (Hohensee *et al.*, 2008).

## 3 RESULTS

### 3.1 LOCALIZATION OF VOLTAGE GATED SODIUM CHANNELS IN THE VENTRAL NERVE CORD AND MN5

In invertebrate neurons and especially monopolar neurons, it is generally unclear where the action potential is generated. In case of monopolar neurons like the MN5, the soma is mostly passive (Duch & Levine 2000; Duch *et al.*, 2008; Meseke *et al.*, 2009) and all of the dendrites originate from a segment defined as the primary neurite. The axon is a continuation of the primary neurite, and it carries the output signal to the flight muscle on the contralateral side. This study investigates the site of action potential generation by combining immunocytochemistry for sodium channels and intracellular staining of MN5 with co-localization analysis.

### 3.1.1 DOCUMENTATION OF SODIUM CHANNEL IMMUNOCYTOCHEMISTRY ALONG THE MN5 NEURITE AND AXON

Sodium channels were detected with the SP19 antibody. SP19 (AB5210) recognizes the  $\alpha$ -subunits in rat type I voltage-gated sodium channels (VGSC). DmNav (formerly *para*) in *Drosophila* encodes the equivalent of the  $\alpha$ -subunit in mammalian sodium channels (Loughney *et al.*, 1989). The predicted *para* polypeptide has the four homology domain structure seen in all other voltage-gated sodium channels (e.g., Guy & Conti, 1990; Hille, 1992) and a high level of amino acid sequence identity with other known sodium channel proteins (Thackeray & Ganetzky, 1994). The specificity of SP19 for insect neurons has been demonstrated in previous studies (French *et al.* 1993; Amat *et al.* 1998; Boerner *et al.* 2006), and it was confirmed in this study via a Western Blot. The inset in Figure 2A shows a band at about ~235 kDa (see white arrow), which corresponds to the predicted size of the DmNav polypeptide in *Drosophila* (UniProtKB/Swiss-Prot: P35500).

Immunocytochemistry staining of SP19 in the ventral nerve cord (VNC) of *Drosophila* was found in axon tracts, commissures, a few unidentified cell bodies, and within nerves exiting the VNC (Figure 2A). For identification of the MN5 axon, the neuron was stained intracellularly. The MN5 staining (Figure 2A, green) could be followed leaving the VNC through nerve II1 (NII1) to its axon terminals on the dorsal longitudinal flight muscle (DLM) fibers five and six. Co-localization of the green MN5 staining with the sodium channel immunocytochemistry staining showed a continuous sodium channel signal along the MN5 axon after exiting the VNC through nerve II1 (Figure 2A, magenta, and white in panel underneath). However, there was only sparse sodium channel staining detectable in the soma or proximal part of the primary neurite.

To further evaluate the onset and distribution of sodium channel staining along the primary neurite and axon, an extensive series of 10  $\mu$ m segments were selected for more detailed inspection and quantification across several animals. The sodium channel signals among these segments were generally consistent across the axon; thus, only a subset of representative segments are shown in depictions and analyses here (Figure 2B and 2C). Relatively little anti-SP19 staining was found in the most proximal segments (51  $\mu$ m from the soma), as depicted in Figure 2B. In the more distant segments, a strong anti-SP19 staining was always present within the MN5 axonal label. For quantitative evaluation, these representative segments were marked by using the Amira LabelField tool (Figure 2A,

white and orange rectangles with numbers representing distance from soma in  $\mu\text{m}$ , 2B, MN5 in green, anti-SP19 in magenta). By utilizing the three-dimensional reconstruction plug-in and co-localization tools in Amira 4.1, it was possible to measure anti-SP19 signal in only those voxels that were found within 100 nm radius (i.e., the same voxel) of the surface of the MN5 intracellular staining. This method was used to quantify the mean co-localized sodium channel staining intensity for each of the selected segments (rectangles in Figure 2A). The procedure was repeated in multiple flies to account for animal variation. Within each animal, the values for each segment were normalized to the segment with the highest staining intensity, and then these relative segment intensities were averaged across all animals (Figure 2C). The number of animals pertaining to each average value is shown for each bar. The segments at a distance of 51  $\mu\text{m}$  from the soma had significantly less staining intensity compared to all the other more distal segments (101  $\mu\text{m}$ , 176  $\mu\text{m}$ , 376  $\mu\text{m}$ , 526  $\mu\text{m}$ , 676  $\mu\text{m}$ , 876  $\mu\text{m}$ ; Figure 2C, ANOVA with Newman Keuls post hoc test,  $p \leq 0.01$ ). Among all segments more distal than 100  $\mu\text{m}$ , no significant difference in staining intensity for sodium channel immunocytochemistry was found (ANOVA,  $p \geq 0.3$ ).

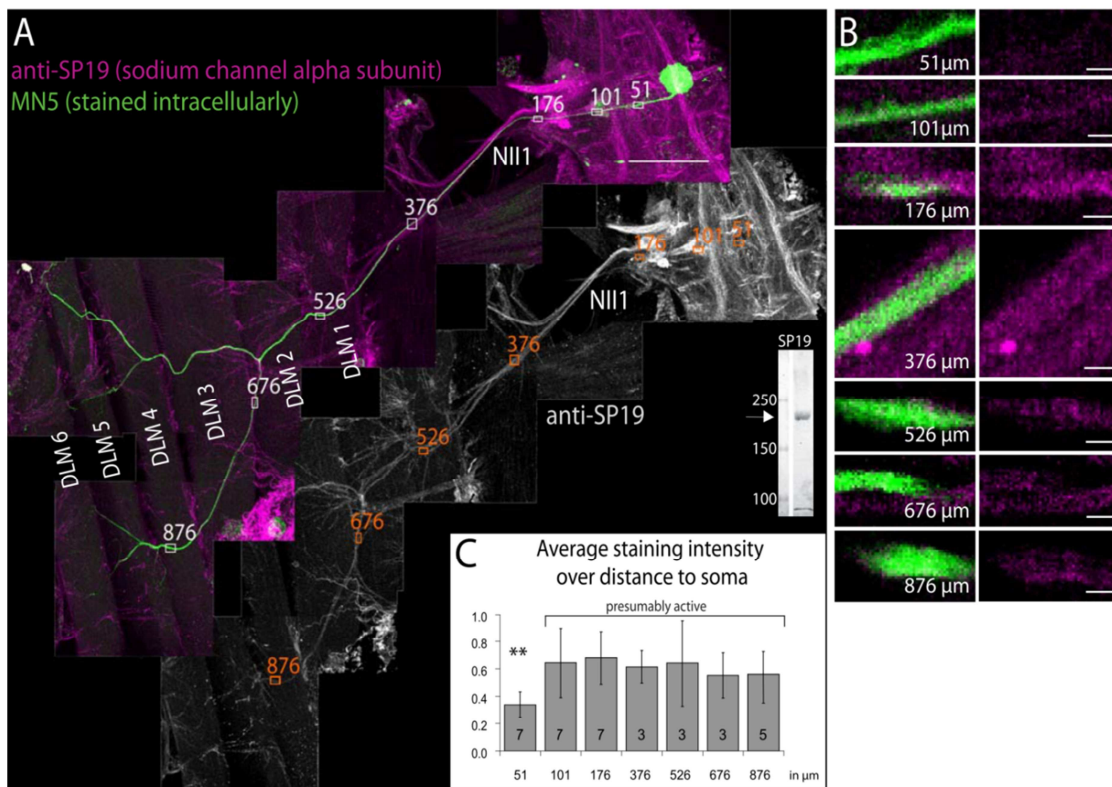


Figure 2: *Sodium Channel Immunocytochemistry Along the MN5 Neurite and Axon in Drosophila*

- A) Montage of several fields of view (projection view) of MN5: in the mesothoracic ganglia, along the nervell1 (NII1), and through the fibers (1-6) of the DLM. Upper montage; sodium channel immunocytochemistry (anti-SP19) in magenta, MN5 intracellular staining in green. Lower montage; sodium channel immunocytochemistry only in grey scale. Within the mesothoracic ganglia, tracts, commissures and a few unidentified cells are stained anti-SP19 positive. The anti-SP19 staining can be also seen in the axon bundles of nerves exiting the VNC and axon terminal branching out over the DLM. Intracellular staining of MN5 can be followed from its soma in the mesothoracic ganglia, along its primary neurite and axon to the contralateral side of the ganglia, exiting through NII1 to the axon terminals, which are branching over DLM fibers 5 and 6. Scale bar 100  $\mu\text{m}$ . Small white and orange rectangles show the locations of the  $\sim 10 \mu\text{m}$  segments of MN5 neurite and axon depicted in (B) and used for longitudinal sampling of staining intensities intensity diagram in (C). The numbers show the distance to the soma in  $\mu\text{m}$ . Inset: Western blot of *Drosophila* thoracic nerve tissue incubated with SP19 antibody (see methods). White arrow signals the band of the recognized protein at about  $\sim 235 \text{ kDa}$ .
- B) Depicts selective enlargements of segments at different locations along the MN5, corresponding to the white and orange rectangles in (A). Sodium channel staining (anti-SP19) in magenta; MN5 intracellular staining in green. Numbers in each picture indicate the distance of the segment from the soma. At a distance of 51  $\mu\text{m}$ , only sparse staining for voltage gated sodium channels (VGSC) was found to be co-localized with MN5. At distance 101  $\mu\text{m}$ , a strong immunolabel for VGSC was detected. All following segments; 176  $\mu\text{m}$ , 376  $\mu\text{m}$ , 526  $\mu\text{m}$ , 676  $\mu\text{m}$ , 876  $\mu\text{m}$  showed VGSC immune positive label with similar intensity co-localizing with the MN5 label. Scale bars: 2  $\mu\text{m}$ .
- C) Quantification of immuno-positive signal of anti-SP19 in seven segments along the primary neurite and axon ( $\sim 10 \mu\text{m}$  each). MN5 neuron reconstructions provided a surface, and only those voxels within 100 nm of that surface were measured for anti-SP19 intensity. Within each animal, the values for each segment were normalized to the segment with the highest intensity. Normalized values were averaged across all animals. The number of animals pertaining to each average is shown in each bar (shown with standard deviation). Only the first bar showing the average of intensities at a distance of 51  $\mu\text{m}$  from the soma is significantly different from the others (ANOVA with Newman Keuls post hoc test,  $p \leq 0.01$ ).

### 3.1.2 ESTIMATING THE SPIKE INITIATION ZONE IN MN5

As described above, average sodium channel immunocytochemistry intensity was the same for axonal segments distal of 100  $\mu\text{m}$ , but the average intensity was significantly lower for segments at 51  $\mu\text{m}$  from the soma. Further analysis of neurite and axonal reconstructions ( $n=7$ ), together with co-localization analysis of sodium channel staining, revealed a sharp increase in sodium channel staining intensity along the section of the primary neurite where the most distal posterior dendrite branches off (Figure 3A, white arrow). One reconstruction is shown as an example in Figure 3A. Red coloration indicates high levels of sodium channel staining, and blue indicates low or no sodium channel staining. For three selected regions, the actual immunocytochemistry stainings are shown below (Figure 3A, region 1, 2, and 3; MN5 intracellular staining in green, sodium channel staining in magenta). Region 2 ( $\sim 60 \mu\text{m}$  from the soma) and 3 ( $\sim 20 \mu\text{m}$  from the soma)

show only a modest amount of anti-SP19 staining signal, and of that small amount, most of it seems to be localized in the cytosol of the MN5 neurite. In region 1 (~90  $\mu\text{m}$  from the soma), however, a strong anti-SP19 staining was detected. Interestingly, the sodium channel staining in region 1 seemed to be concentrated around the edges of the MN5 intracellular staining (Figure 3A, white asterisks), which suggests that most of the stained protein may be localized in the MN5 membrane rather than being suspended in the cytosol.

Among the seven animals tested, a sharp increase in sodium channel staining intensity was found on average at  $88 \pm 15$   $\mu\text{m}$  distance from the soma. For the development of a method enabling the prediction of the site of sudden sodium channel intensity increase in animals without sodium channel immunocytochemistry, the distal-posterior sub-tree was chosen as a landmark (Figure 3B, 3C, blue dendrite). This sub-tree could be identified between animals due to its characteristic shape and position within the MN5 dendritic tree (Vonhoff & Duch, 2010). In the seven animals tested this most distal-posterior sub-tree was located on average at a distance of  $91 \pm 17$   $\mu\text{m}$  from the soma. The distances between distal-posterior sub-tree and the observed point of sudden sodium channel intensity increase were measured for seven animals. The average of these measurements yielded a factor of 0.97 with a standard deviation of  $\pm 0.116$ , describing the relationship between these two points. Applying these values to individual MN5 cells allowed for the estimation of an interval where the sudden increase in sodium channel intensities was most likely. If the interval was set to approximately  $11 \pm 3$   $\mu\text{m}$  (average value) around the most distal posterior sub-tree of MN5, it was possible to predict with 70 percent accuracy the observed border of low to high VGSC intensity in the seven MN5 reconstructions tested. Figure 3B and 3C show two representative MN5 dendritic tree reconstructions for which this method yielded an accurate estimate of the putative spike initiating zone (SIZ). The most distal dendritic tree is depicted in blue. The red dotted lines show the proximal half of the calculated interval in which sodium channel intensity increase may be observed (Figure 3B, interval spans  $11.25$   $\mu\text{m}$ , and in 3C  $12.1$   $\mu\text{m}$ ). The whole interval is marked in red on the MN5 neurite itself. The part of the MN5 that is distal of this interval and hence should most definitely have high VGSC staining intensities (see Figure 2) is marked in orange. In both examples, the region in which sodium channel intensity increase is most likely is located at the distal end of the primary neurite of MN5, at a region where the most distal dendrites are branching off. Within the limitations of this method, the site of action potential generation can be

estimated in MN5 reconstructions without an additional sodium channel staining (see discussion).

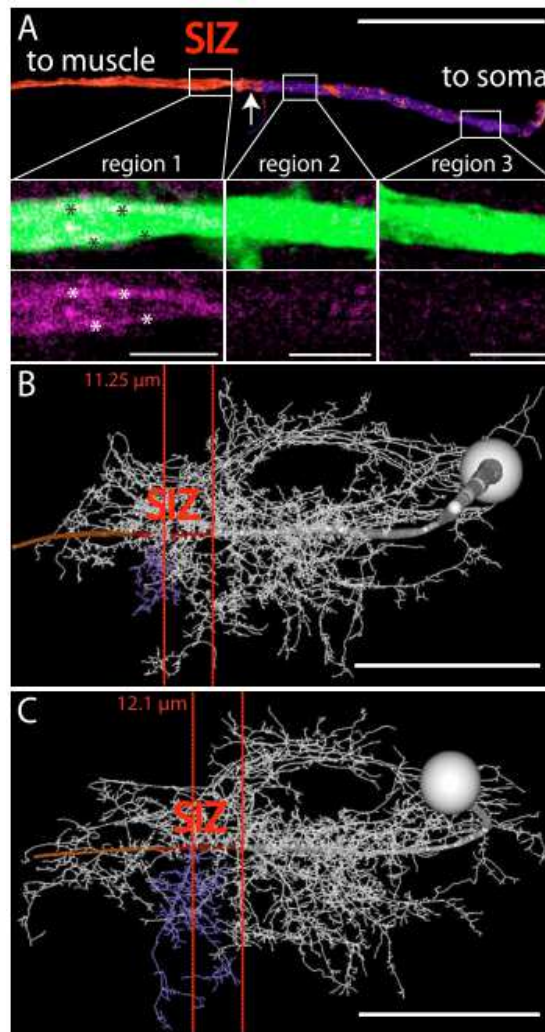


Figure 3: *Estimation of the spike initiating zone (SIZ) in MN5.*

- A) Depicts a partial surface reconstruction of the MN5 primary neurite, with the soma laying on the right side and the axon leading out of the VNC to the muscle on the left side. Reconstruction is false color coded with respect to sodium channel staining intensity co-localizing with MN5 surface reconstruction; red and blue indicate high and low staining intensities, respectively. White arrow points to the spot where a sharp increase in sodium channel immunostaining intensity was observed. White rectangles show the location on the MN5 for selected enlargements (single optical sections) of VGSC immunostaining (magenta) and MN5 intracellular staining (green). Regions 2 (~60 $\mu$ m from the soma) and 3 (~20 $\mu$ m from the soma) show relatively little immunostaining for VGSC, which seems to be localized mostly within the MN5 staining. Region 1 (~90  $\mu$ m from the soma) shows a strong immunopositive staining, which seems to be localized mainly near the membrane of the MN5 label, indicated with white asterisks. Scale bars: 50  $\mu$ m in top frame, 5  $\mu$ m in enlargements.
- B,C) Full reconstructions of the MN5 dendritic tree (spheres model) with parts of the axon and the soma. The most distal posterior subtree is shown in blue. The region where VGSC exhibits a sharp increase, and hence, where action potential initiation is most likely, is

shown in red. MN5 reconstruction distal of that region is shown in orange. Red dotted vertical lines indicate the half of the region proximal to the most distal posterior subtree. In case of the neuron depicted in (B) it has a length of 11.25  $\mu\text{m}$ . In (C) the interval has a length of 12.5  $\mu\text{m}$ . Scale bars: 50  $\mu\text{m}$ .

## 3.2 DISTRIBUTION PATTERNS OF PUTATIVE CHOLINERGIC AND GABAERGIC INPUT SYNAPSES ON THE MN5 DENDRITIC TREE

To unravel the mechanisms of neuronal communication, it is critical to understand both where information enters the cell and where that information is converted into an output signal. The latter question was addressed in chapter 3.1, where the putative region for action potential generation was examined and estimated. Chapter 3.2 presents this study's findings pertaining to the former question, investigating where information enters the motoneuron MN5 with regard to the estimated spike initiating zone (SIZ). Chapter 3.2.1 will focus on putative cholinergic input sites and chapter 3.2.2 emphasizes putative GABAergic input sites.

### 3.2.1 LOCALIZATION OF PUTATIVE CHOLINERGIC INPUT SYNAPSES ON MN5 DENDRITES

The majority of fast excitatory transmission in invertebrates is facilitated by nicotinic acetylcholine receptors (nAChRs). In all neurons of the *Drosophila* escape circuit, including MN5, the  $D\alpha 7$  subunit of the nAChR is expressed abundantly (Fayyazuddin *et al.*, 2006). It can therefore be assumed that large parts of MN5's cholinergic input will be mediated through this type of receptor. This chapter will address the question of whether cholinergic inputs are distributed evenly, or if they are targeted to specific sub-domains on the MN5 dendritic tree. To visualize the  $D\alpha 7$  subunit of nAChR, a previously described UAS- $D\alpha 7$ -GFP construct (Raghu *et al.*, 2009) was expressed under the control of P103.3-GAL4, which expresses in several motor neurons, including MN5 (Consoulas *et al.*, 2002). The expression pattern was visually analyzed and compared to an antibody staining against  $D\alpha 7$  nAChR. The antibody staining displayed a punctuated pattern. Higher

densities were found in regions containing flight motoneuron dendrites, including MN5, as it was previously described by Fayyazuddin *et al.* (2006) (Figure 4A-D).  $D\alpha 7$  expression driven under the control of P103.3-GAL4 also showed a distinct and punctuated pattern in the MN5 dendritic field. In both cases (anti-AChR and P103.3xnAChR-GFP), the punctuated staining for  $D\alpha 7$  nAChR overlapped with individual dendrites of MN5 (Figure 4C, 4G). Taken together, these results suggest that P103.3-GAL4 is an appropriate driver line to restrict  $D\alpha 7$  expression to a limited number of motor neurons, including MN5. Consequently,  $D\alpha 7$  expression under the control of P103.3 was used together with an MN5 intracellular staining for further analysis of synaptic distribution patterns. In addition, a staining for NC82 was added to mark putative pre-synaptic sites. MN5 intracellular staining was used to prepare three-dimensional surface reconstructions, onto which the putative cholinergic input synapses could be mapped and analyzed (for more details see methods; Evers *et al.*, 2005; Schmitt *et al.*, 2004). The criteria for a positive count on the MN5 surface reconstruction required that the  $D\alpha 7$  signal and the MN5 surface had to overlap, and that this overlap also had to be in close proximity (300nm) to a NC82 label (as shown in Figure 4G, 4H).

Visual analysis of MN5 surface reconstructions (n=5) with putative cholinergic synapse mapping revealed that putative cholinergic synapses were found on all dendrites of the MN5. However, the highest concentration of cholinergic synapses was observed in the half of the MN5 dendritic tree proximal to the soma (Figure 5B, white circle). Lowest densities were found in the distal half of the dendritic tree and anterior of the estimated spike initiating zone (SIZ) (Figure 5B, white arrow 2). MN5 dendrites originating at the SIZ and arching toward the MN5 soma were also mostly lacking putative cholinergic synapses (Figure 5B, white arrow 1).

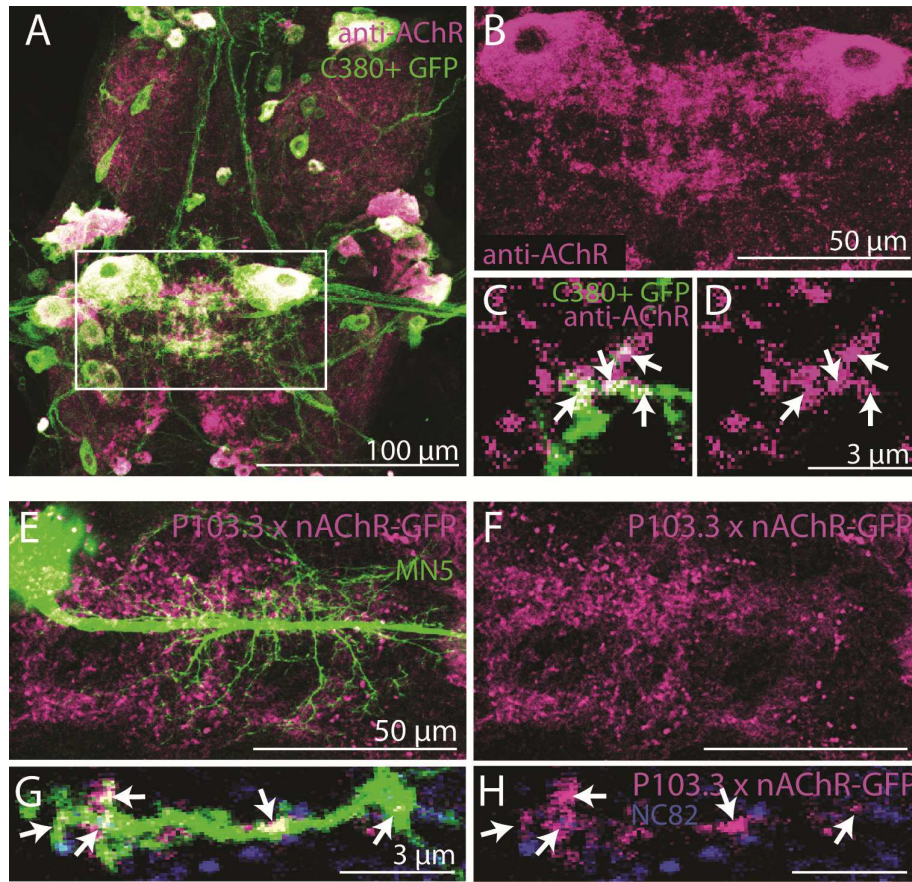


Figure 4: *Da7* Localization in the Neuropil of the Adult Mesothoracic Ganglia of *Drosophila melanogaster*.

- A) Projection view of double-label immunohistochemistry for  $\text{Da7}$  nAChRs (magenta) and GFP (green) under the control of the motoneuron driver C380-GAL4;Cha-GAL80 in the ventral nerve cord of *Drosophila*. Co-localization appears white. White rectangle demarks the localization for both left and right MN5 somata.
- B) Projection view. Selective enlargement of  $\text{Da7}$  nAChRs immunolabel from white rectangle in (A). MN5 somata are  $\text{Da7}$  positive, and punctuated  $\text{Da7}$  label is found throughout the neuropil region that contains MN5 dendrites.
- C) Representative enlargement of a single optical section from within the motor neuron dendritic field. Motor neuron processes are depicted in green, anti-nAChR in magenta, and the overlap of the two stainings in white. White arrows point to examples of overlap between motor neuron processes and anti-nAChR.
- D) Same enlargement as shown in (C), showing anti-nAChR staining only. White arrows demark the same points as in (C).
- E) Intracellular staining of MN5 (green) superimposed on  $\text{Da7}$ -GFP label (magenta) in a representative animal with UAS- $\text{Da7}$ -GFP expression under the control of the motoneuron driver P103.3-GAL4. Punctuated  $\text{Da7}$  label in neuropil appears similar following overexpression of GFP tagged  $\text{Da7}$  receptors (E, F) and following immunohistochemistry for native  $\text{Da7}$  protein in the flight motor neuropil in adult flies (A, B).
- F)  $\text{Da7}$ -GFP label from (E) alone without MN5 intracellular staining, shown for better comparison.
- G) Selective enlargement of a single optical section containing one MN5 dendritic branch (green) and  $\text{Da7}$ -GFP puncta (magenta). Overlap of MN5 dendrite staining and  $\text{Da7}$ -GFP puncta appear white and are demarked by arrows.

- H) Same optical section as in (D) but only D $\alpha$ 7-GFP puncta (magenta) and anti-NC82 puncta (presynaptic marker, in blue) are shown. D $\alpha$ 7-GFP puncta that were co-localized with MN5 dendrite as shown in (G) are directly adjacent to NC82 positive presynaptic terminals.

The next approach was to determine whether individually identified sub-domains of the adult MN5 dendritic tree (defined as sub-trees by Vonhoff & Duch, 2010) contain similar amounts of cholinergic synapses, or if they are preferentially targeted to specific sub-trees. Vonhoff and Duch (2010) defined 23 sub-trees in MN5. To calculate the proportion of putative cholinergic synapses found on each sub-tree relative to all putative cholinergic synapses found on the whole dendritic tree, the number of positively scored triangles on each sub-tree was divided by the sum of all such positively scored triangles throughout the whole dendritic tree. All 23 sub-trees were ranked according to these percentage estimates. On average,  $10 \pm 2$  sub-trees out of 23 sub-trees contained 75 percent of all putative cholinergic synapses in a single cell. To visualize the position of these sub-trees within the whole dendritic tree, the sub-trees were color-coded using colors from a heatmap (depicted in Figure 5D), as it is shown for the four example reconstructions in Figure 5C-F. The sub-tree with the highest proportion of putative cholinergic synapses (14 percent on average) was always colored in red. All sub-trees with lower percent values received colors ranging from orange to yellow to white. On average, white colored sub-trees (lowest in ranking) contained 5 percent of the total cholinergic staining. Sub-trees that were not included in the 75 percent group were colored in black. Note that colors do not correlate to specific percent values and are only used to visualize the ranking of the sub-trees within each of the analyzed MN5 reconstructions. Interestingly, this analysis reveals that the sub-tree with the highest proportion of putative cholinergic input is often located near the center or the proximal half of the MN5 dendritic tree (Figure 5B, white arrow). Moreover, the majority of sub-trees in this 75 percent group were located in the half of the dendritic tree proximal to the soma (Figure 5C-F, white circle). In contrast, all of the sub-trees in the distal-posterior region of the MN5 dendritic tree, and most in the distal-anterior region, contained less than 5 percent of the total putative cholinergic input, and they were therefore colored in black (Figure 5C-F). These findings support the initial observation that most of the putative cholinergic input is indeed located in the half of the dendritic tree that is proximal to the soma of MN5.

Further quantifications of the distribution of putative cholinergic synapses throughout the MN5 dendritic tree were made with regard to branch order and distance to the spike initiating zone (SIZ). Branch order and distance are critical parameters influencing signal propagation in complex dendritic trees. The complex dendritic tree of MN5 entails more than 6500  $\mu\text{m}$  total length and more than 4000 branches (Vonhoff & Duch, 2010). For morphometric analyses, the section of the primary neurite that was identified as SIZ was set as origin. Therefore, all branches originating from that segment were first order branches. Distance values are measured as the path length from the 0 order branch of the sub-tree along the midlines of the reconstruction. With the SIZ set as tree origin, 95 percent of all branches belong to branch order  $58 \pm 10$  and lower. Densities for one particular branch order were averaged among all branches with the same branch order (Figure 5G). As a result, putative cholinergic synaptic inputs were found on all branch orders. In branch orders up to  $58 \pm 10$ , between 4 to 9 percent (average of 6 percent) of the dendritic surface were positive for putative cholinergic input (Figure 5G). In four out of five preparations, branch orders above  $58 \pm 10$  contained higher densities (11 percent on average). However, it should be noted that only 5 percent of all dendritic branches fall in this category. Therefore, the total surface area pertaining to these branch orders (58 and higher) is relatively small, and hence few positively scored inputs will have a much stronger effect on density values. To account for branch order variation among all five animals, branch orders were normalized in each animal to their highest branch order (Figure 5H). The motivation for this analysis was to determine whether cholinergic synapses tend to localize on lower, and therefore more proximal, or higher, and therefore more distal, branch orders with respect to the spike initiating zone. For simplicity, normalized branch order bins can be reviewed and will be discussed by quarters. Branch orders pertaining to the two most proximate quarters, which contain the lowest branch orders, had on average 5 percent of their surface counted positive for putative cholinergic input. The third quarter, which contains intermediate to higher order branches, had a mean density of 8 percent. Lastly, the fourth quarter, which included the higher order branches but also contained the least number of branches, had an average density of 11 percent. Therefore, when interpreting branch order data it is important to note that the second and the third quarters contain most of the dendritic branches and hence most of the surface area of the MN5 dendritic tree. Consequently, positively scored surface triangles in these two quarters are measured against a much higher total surface area, which results in lower density values. This relationship between total surface area

(total number of triangles), surface area counted positive for cholinergic input (nAChR positive triangles), and the percent density (positive nAChR triangles divided by total surface area triangles) is depicted in Figure 5K. A parallel increase in total surface area and number of triangles that were scored positive for putative cholinergic input results in a low density value for most branches (quarters one through three). The increase in density values toward the most distal branch orders is the result of a rapid decline in the total number of triangles compared to the number of triangles scored positive for putative cholinergic input. The graphical representation clearly shows that most of the putative cholinergic input is distributed among branches of intermediate order (normalized branch orders 0.45-0.7, quarters two and three). Relatively little putative nAChR is located on the branches of the highest orders, but those branches possess only a small surface area (Figure K).

In summary, most of the putative cholinergic input was not found on branches of the lowest or highest orders, but on intermediate branch orders. Interestingly, these intermediate branches are so numerous that they comprise most of the dendritic tree's surface. Therefore, the majority of cholinergic input is distributed widely with relatively low density among the many branches comprising most of the surface area of the MN5 dendritic tree. Higher density values were only found at the few highest order branches, which comprise only a small portion of the MN5 dendritic surface area.

Similar to the branch order analysis described above, the putative cholinergic synapse distribution was also assessed according to tree distance from the SIZ. First, the entire dendritic tree was divided into 2  $\mu\text{m}$  segments measured by tree distance from the SIZ. Then, the density of nAChR positive triangles was calculated for each segment. Finally, all 2  $\mu\text{m}$  segments were binned according to their distance from the SIZ, and the density values within each bin were averaged. Figure 5I shows this data with different colored lines for each of the five animals analyzed (note that maximum recorded tree distance varied from 80 to 130  $\mu\text{m}$ ). At distances 1 to 60  $\mu\text{m}$  from the SIZ, putative cholinergic synapses were found in densities ranging between 2 to 18 percent in all five animals analyzed. At distances higher than 60  $\mu\text{m}$ , two out of five animals showed higher densities (14 to 23 percent) of putative cholinergic synapses. The most distal dendrites (distances >100  $\mu\text{m}$ ) of MN5 showed only low densities or were completely devoid of putative cholinergic input.

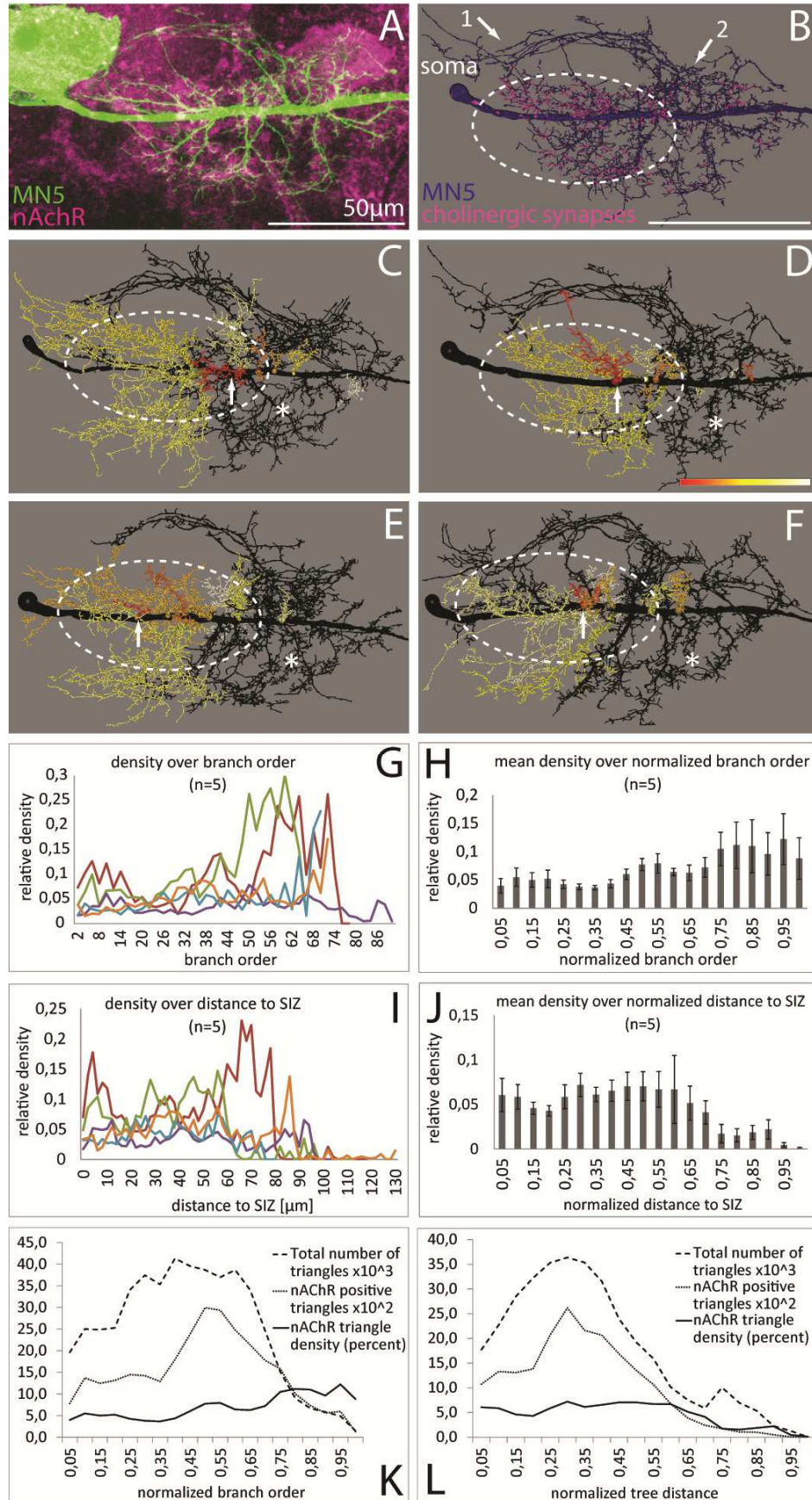


Figure 5: *Distribution of Putative Cholinergic Inputs to the  $\alpha 7$  nAChR Through MN5 Dendrites*

- A) Representative projection view of intracellular staining of MN5 (green) and GFP-tagged  $\alpha 7$  receptors following expression of  $\alpha 7$ -GFP under the control of P103.3-GAL4.
- B) Mapping of  $\alpha 7$ -GFP puncta that are co-localized with MN5 dendrites and within 300nm of NC82 puncta (see methods) onto the surface reconstruction of MN5 (blue). Positively scored  $\alpha 7$ -GFP triangles are in magenta. Soma is located on the left side and the axon would be leaving to the right.
- C-F) Four different surface reconstructions are shown in the same orientation as shown in (A) and (B) Scale bar: 50  $\mu\text{m}$ . Individual sub-trees (defined by F. Vonhoff, after Vonhoff & Duch, 2010) were ranked in a descending order, according to their total percent amount of positive putative cholinergic counts with respect to the total amount of putative cholinergic inputs of the whole dendritic tree. The sub-trees pertaining to 75 percent of the total amount of putative cholinergic inputs were colored. The colors were chosen from a heat map, shown in (D). The sub-tree with the highest percent amount was colored in red and the one with the lowest was colored white. Sub-trees containing percent amounts in-between were given colors according to their ranking from red, orange, yellow to white. Therefore, the colors seen in C-F do not correspond to specific percent values of putative cholinergic input, but rather visualize the position of the sub-tree in the ascending ranking, showing only sub-trees pertaining to the 75 percent of total putative cholinergic inputs. Sub-trees that do not count toward the 75 percent and that were hence lower in the ranking were colored in black. White circle depicts the area in which most of the higher ranked sub-trees are located and hence most of the putative cholinergic inputs are located. White arrow points to the sub-tree with the highest percent amount of cholinergic input in a cell. White asterisks indicate the distal posterior area, where low putative cholinergic input concentration was observed.
- G) Average density of positively scored  $\alpha 7$ -GFP triangles on MN5 dendrites over branch order for 5 representative animals. For branch order definition the putative SIZ was defined as tree origin.
- H) Relative density of positively scored  $\alpha 7$ -GFP triangles on MN5 dendrites normalized to highest order branch in each animal, shown with standard deviation.
- I) Average density of positively scored  $\alpha 7$ -GFP triangles on MN5 dendrites over distance to putative SIZ.
- J) Relative density of positively scored  $\alpha 7$ -GFP triangles on MN5 dendrites normalized to highest distance branch in each animal, shown with standard deviation. Significant difference found in normalized density values between anterior and distal groups (ANOVA, Newman Keuls post hoc test  $p < 0.01$ ).
- K,L) Depicts averages ( $n=5$ ) of total number of triangles, total number of triangles positively scored for putative cholinergic input, and percent density of putative cholinergic input over normalized branch order and normalized tree distance.

For comparison among all five animals, distances were normalized to their highest distance in each animal before an average was calculated across all animals (Figure 5J). Data are shown in 5 percent bins. The putative nAChR density remained relatively constant for the first 75 percent of each animal's dendritic tree, with an average of 6 percent (Figure 5J). This corresponds to the first  $82 \pm 14 \mu\text{m}$  of tree distance from the SIZ. In contrast, the segments in the most distal 25 percent of each tree only contained putative nAChR density values of 1 percent, on average. This latter 25 percent

corresponds to tree distances in the range of 84-130  $\mu\text{m}$  from the SIZ and most likely include the dendrites forming an arch towards the soma. Figure 5L shows the relationship between total number of surface triangles, positively scored triangles, and the resulting density values for putative cholinergic input. Similar to the distribution pattern described with respect to branch order, most of the putative cholinergic input localizes on dendrites that comprise most of the dendritic tree's total surface, and they are located in the second and third quarter of all distances. Therefore, most putative cholinergic input is localized at an intermediate distance. Notably, most distal dendrites had a low density. Since dendrites pertaining to the highest branch order bins were found to have the highest densities for putative cholinergic input (see above), it can be concluded that the most distal dendrites are not included among the dendrites with the highest branch orders.

In summary, the analysis of branch order and distance with respect to the spike initiating zone (SIZ) revealed that, on average, most dendrites of the adult MN5 dendritic tree exhibited relatively low densities of about 6 percent for putative cholinergic input. The highest quantities of putative cholinergic input were distributed on dendrites of intermediate branch order and distance. However, the highest density of putative cholinergic input was found on higher order branches. On the other hand, the segments that were furthest from the SIZ, which most likely include the dendrites forming an arch towards the soma, were mostly devoid of putative cholinergic synapses. The analysis of individual sub-trees revealed that putative cholinergic synapses are preferentially located on  $10 \pm 2$  identified sub-trees, and those sub-trees constitute the proximal half of the dendritic tree, relative to the soma. Moreover, sub-trees originating at or near the SIZ, which is located at the distal end of the primary neurite, were mostly devoid of putative cholinergic input.

### ***3.2.2 LOCALIZATION OF PUTATIVE GABAERGIC INPUT SYNAPSES ON MN5 DENDRITES***

GABA<sub>A</sub> receptors (GABA<sub>A</sub>-R) are the predominant receptor used for the mediation of fast inhibitory transmission in invertebrate nervous systems. Rdl is well characterized and abundantly expressed in the *Drosophila* brain and ventral nerve cord (Harrison *et al.*, 1996; Liu *et al.*, 2007, Agosto *et al.*, 2008, Raghu *et al.*, 2007). It is therefore assumed to

play a major role in the mediation of inhibitory transmission in MN5. This chapter will discuss whether putative GABA<sub>A</sub>-Rs are distributed uniformly or in distinct patterns onto dendrites of the MN5.

To visualize GABA<sub>A</sub>-R, a HA-tagged Rdl construct (Sánchez-Soriano *et al.*, 2005; Raghu *et al.*, 2007) was expressed under the control of C380-GAL4 to restrict expression to only a subset of thoracic neurons, including MN5 (Duch *et al.*, 2008). The pattern yielded by the expression of HA-Rdl under the control of C380-GAL4 was compared to the native pattern of Rdl receptors on dendrites of the adult MN5 using immunocytochemistry. Visual evaluation revealed a similar pattern of distinct puncta in the MN5 dendritic field (Figure 6A and 6B, compare to 6G and 6H). Anti-Rdl label combined with C380-GFP expressed in several motor neurons (Consoulas *et al.*, 2002) shows that there is significant overlap between the GFP marked dendrites and the labeled receptors (Figure 6A, 6C). Additionally, overlapping C380-GFP and anti-Rdl staining could be found adjacent to presynaptic NC82 staining (Figure 6 C-F, white arrows). Rdl expression was paired with MN5 intracellular staining. Only Rdl positive puncta overlapping with MN5 intracellular staining were counted as positive on MN5 surface reconstructions, as shown in Figure 6D and 6E (see methods, Evers *et al.*, 2005, Schmitt *et al.*, 2004). Unfortunately, a triple staining between MN5 and Rdl together with the presynaptic marker NC82 was not possible because of the cross-recognition of antibodies (see methods). Based on the visual comparison between the Rdl-HA expression pattern and the antibody staining of the native Rdl pattern, as well as extensive evaluations and descriptions of the Rdl-construct in previous papers, it was confidently assumed that a C380-GAL4 driven expression of the Rdl-HA construct, combined with MN5 intracellular staining, was an appropriate method to test for distribution patterns of putative GABA<sub>A</sub>-R on MN5 dendrite reconstructions.

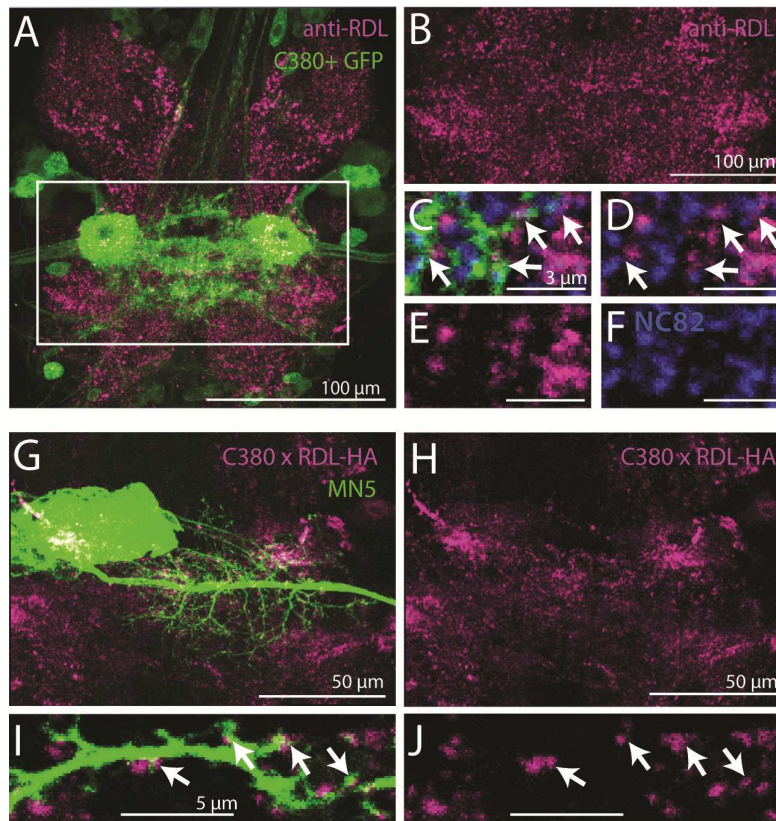


Figure 6: *Rdl* Localization in the Neuropil of the Adult Mesothoracic Ganglia of *Drosophila melanogaster*

- A) Projection view of double-label immunohistochemistry for Rdl GABA<sub>A</sub>-Rs (magenta) and GFP (green) in the ventral nerve cord of animals expressing UAS-GFP under the control of the motoneuron driver C380-GAL4;Cha-GAL80. Co-localization appears white. White rectangle demarks the localization of both left and right MN5 somata.
- B) Projection view. Selective enlargement of Rdl GABA<sub>A</sub>-R immunolabel from white rectangle in (A). Punctuated Rdl label is found throughout the neuropil region that contains MN5 dendrites.
- C) Representative enlargement of a single optical section from within the motor neuron dendritic field. Motor neuron processes stained in green, anti-Rdl in magenta, NC82 presynaptic marker in blue, overlap of the three stainings in white. White arrows point to examples of overlap between motor neuron processes, anti-Rdl and NC82.
- D-F) Same enlargements as shown in (C), showing anti-Rdl staining only in (D), anti-RDL only in (E), anti-Rdl and NC82 in (F). White arrows in (D) demark the same points as in (C).
- G) Projection view. Intracellular staining of MN5 (green) superimposed on Rdl-HA label (magenta) in a representative animal with UAS-Rdl-HA expressed under the control of the motoneuron driver C380-GAL4. Punctuated Rdl label in neuropil appears similar following overexpression of HA tagged Rdl receptors (G, H) compared with immunohistochemistry for native Rdl protein in the flight motor neuropil (B).
- H) Rdl-HA label only as shown in (G).
- I) Selective enlargement of a single optical section containing one MN5 dendritic branch (green) and Rdl-HA puncta (magenta). Overlap of MN5 dendrite staining and Rdl-HA puncta appear white and are demarked by arrows.
- J) Same optical section as in (I) but shown are only anti-Rdl-HA puncta.

The analysis of putative GABAergic synapse distribution on the MN5 dendritic tree was performed in a similar routine as described for putative cholinergic synapses to allow a comparison between these two antagonistically acting input synapses. Visual analysis of MN5 surface reconstructions (n=5), in tandem with mapped putative GABAergic synapses, revealed higher concentrations in an area near the estimated SIZ and at the most distal end of the dendrites forming an arch toward the soma (Figure 7B, white circles). Both the proximal half and, especially, the posterior half of the dendritic tree seemed to contain lower concentrations of putative GABAergic synapses relative to the anterior-distal region (Figure 7B, white circle). However, no area of the MN5 dendritic tree seemed to be completely devoid of putative GABAergic synapses.

The next objective was to determine whether individual sub-trees contain similar amounts of putative GABAergic synapses, or if they are preferentially targeted to specific sub-trees. The number of positive triangles on each sub-tree, relative to the number of positive triangles on the whole dendritic tree, was calculated in the same manner as employed for putative cholinergic input analysis (chapter 3.2.1). The sub-trees were ranked according to this percentage for putative GABAergic input, and the subset of trees pertaining to 75 percent of all positive triangles were color coded following the same rules as described above (Figure 7C-F, red indicates the sub-tree with the highest percent, white the lowest, and sub-trees not counting toward the 75 percent are colored in black). On average, the top 7 out of 23 sub-trees contained 75 percent of all putative GABAergic input synapses. Furthermore, sub-trees containing the highest percent of putative GABAergic input were primarily located in the anterior-distal portion of the MN5 dendritic tree (Figure 7C-F, red and orange colored sub-trees), and in most preparations these include the long dendrites forming an arch toward the soma. The sub-tree with the highest percent concentration (on average 12 percent) for putative GABAergic inputs was in four out of five cases directly branching off the SIZ (Figure 7C, 7D, 7F, white arrow). In one case, the sub-tree with the highest percentage concentration of putative GABAergic input was found on a sub-tree located more proximal to the soma. However, the sub-tree containing the second highest percent value was again located where the SIZ was estimated (Figure 7D, white arrow).

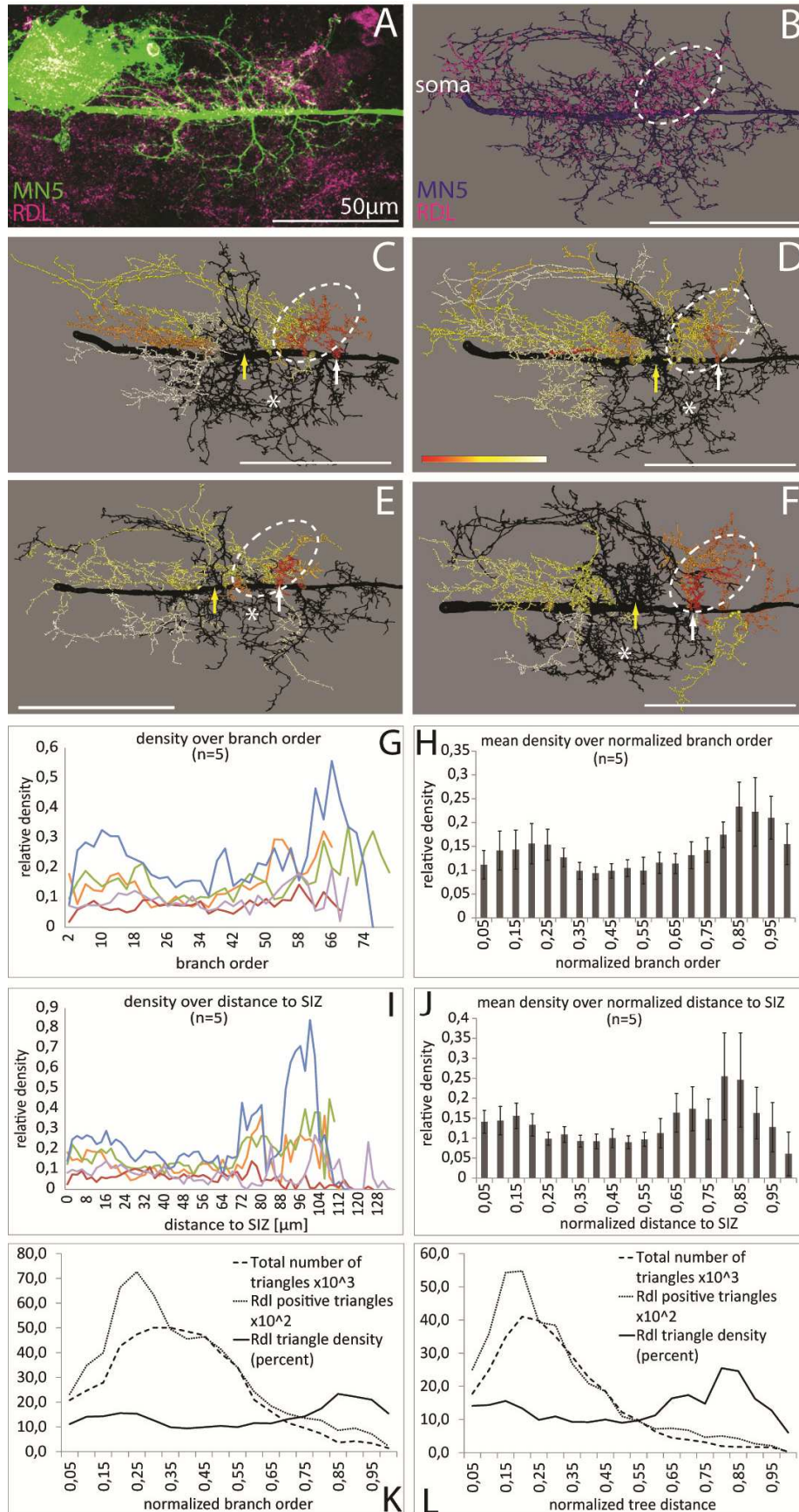


Figure 7: *Distribution of Rdl GABA<sub>A</sub>R- on MN5 Dendrites indicating Putative GABAergic Inputs*

- A) Representative projection view of intracellular staining of MN5 (green) and HA-tagged GABA<sub>A</sub> receptors following expression of Rdl-HA under the control of C380-GAL4.
- B) Mapping of Rdl-HA puncta that are co-localized with MN5 dendrites onto the surface reconstruction of MN5 (blue). Positively scored Rdl-HA triangles are in magenta. Soma is located on the left side and the axon would be leaving to the right.
- C-F) Four different surface reconstructions are shown in the same orientation as shown for (A) and (B) Scale bar: 50  $\mu$ m. Individual sub-trees (defined by F. Vonhoff, after Vonhoff & Duch, 2010) were ranked in a descending order, according to their total percent amount of positive putative GABAergic counts with respect to the total amount of putative GABAergic inputs of the whole dendritic tree. The sub-trees pertaining to 75 percent of the total amount of putative GABAergic inputs were colored. The colors were chosen from a heat map, shown in (D). The sub-tree with the highest percent amount was colored in red and the one with the lowest was colored white. Sub-trees containing percent amounts in-between were given colors according to their ranking from red-orange over yellow to white. Therefore, the colors seen in C-F are not corresponding to specific percent values of putative GABAergic input, but rather visualize the position of the sub-tree in the ascending ranking, showing only sub-trees pertaining to the 75 percent of total putative GABAergic inputs. Sub-trees that do not count toward the 75 percent and that were hence lower in the ranking and contained lower percent amount of putative GABAergic inputs, were colored in black. Sub-tree Sub-tree White circle depicts the area in which most of the higher ranked sub-trees are located and hence most of the putative GABAergic inputs are located. White arrow points to the sub-tree with the highest percent amount of cell. Yellow arrow points to the center of the whole dendritic tree, which is mostly devoid of putative GABAergic inputs. White asterisks indicate the posterior region of the dendritic tree, where low putative GABAergic input concentration was observed.
- G) Relative density of positively scored Rdl-HA triangles on MN5 dendrites over branch order for 5 representative animals. For branch order definition the putative SIZ was defined as tree origin.
- H) Average density of positively scored Rdl-HA triangles on MN5 dendrites over normalized branch order. Normalized to highest order branch in each animal, shown with standard deviation.
- I) Relative density of positively scored Rdl-HA triangles on MN5 dendrites over distance from the putative SIZ for 5 representative animals.
- J) Average density of positively scored Rdl-HA triangles on MN5 dendrites over normalized distance to putative SIZ. Normalized to highest distance branch in each animal, shown with standard deviation.
- K,L) Depicts averages (n=5) of total number of triangles, total number of triangles positively scored for putative GABAergic input, and percent density of putative cholinergic input

Interestingly, the center of the dendritic tree, and most of the posterior portion of the dendritic tree, were not included among the top 75 percent, and hence, these regions include only sub-trees with a lower amount (less than 5 percent on average) of putative GABAergic synapses (Figure 7C-F, yellow arrow, white asterisks). These results therefore support the findings from the visual analysis discussed above.

Similar to the analyses on putative nAChRs, quantification of the distribution of putative GABAergic input was conducted with regard to branch order and distance. The

SIZ was again set as origin for statistical analyses, and the densities pertaining to the same branch order or tree distance bin were averaged. Putative GABAergic input was found on all branch orders, ranging between 2 to 34 percent. Branch orders 51±7 and lower contained 95 percent of the whole dendritic surface area in the 5 cells analyzed. These dendrites were found to have a mean putative GABA<sub>A</sub>-R density of 12 percent. The remaining 5 percent of the dendritic surface contained mostly higher order branches and had an average density of 20 percent. Overall, a slight tendency of higher density values among both the lower (1 to 45 branch order) and higher branch orders (45 to 80 branch orders) was observed (Figure 7G). Thus, the bimodal distribution observed through visual inspection (Figure 7B), with a higher concentration of putative GABAergic input on dendrites close to the SIZ and on the very long dendrites growing in an arch toward the soma, seems to be reflected in this quantitative analysis as well.

After normalizing the branch order of each reconstruction to their highest branch order, densities for all five animals analyzed were averaged. Once more, the motivation was to examine if putative GABAergic input is distributed evenly throughout the dendritic tree, or if it is targeted to specific branch orders. Similar to the evaluation of nAChRs distribution patterns, the density values for the normalized dendritic branch orders were assessed by quarters. The mean densities for the first and the last quarter were found to be the highest. The first quarter, which comprises mostly lower branch orders, close the SIZ had a mean density of 14 percent. The mean density for the last quarter was 20 percent and therefore a lot higher. However, it must be noted that fewer branches pertain to the last quarter, and hence a few positively scores triangles on only a few branches have a much greater impact on density values (Figure 7K). The middle two quarters, which comprise most of the dendritic branches, had only 10-12 percent of their surface scored positive for putative GABAergic input. The relationship between total surface area (total number of triangles), surface area scored positive for putative GABAergic input (total number of Rdl positive triangles), and their resulting density values are depicted in Figure 7K, all of which are measured across normalized branch-order bins. Similar to the last quarter, the high densities reported for the first quarter are the result of high amounts of positively scored triangles found on relatively few branches. The peak number of positively scored triangles can be found at the boundary between quarter one and two. Densities for quarter two decrease because the number of positively scored triangles decreases and the surface area pertaining to this quarter increases. Although the number of positively scored triangles remains relatively high, their

wider distribution over a larger surface area yields comparatively low density values for each branch order bin. The highest density was found in the last quarter. As shown in Figure 7K, the increase in density is due to a steeper decrease in total surface area compared to the surface that was scored positive for putative GABAergic input. Therefore, a smaller number of positively scored triangles are now distributed on a considerably decreased surface area, and thus a few positively scored triangles have a much greater effect on density values.

In summary, putative GABAergic inputs are not restricted to higher or lower order dendrites only. However, the majority of putative GABA<sub>A</sub>-Rs were found on lower order branches, which are close to the SIZ. Additionally, the highest density was found on the higher order branches, farthest from the SIZ.

Analysis of putative GABA<sub>A</sub>-R densities with respect to tree distance to the SIZ revealed a similar bimodal distribution to the pattern described for branch-order analyses above (Figure 7L). Dendrites closest and farthest from the SIZ showed higher density values for putative GABAergic input (Figure 7I). However, the highest amounts of putative GABAergic inputs were found on dendrites close to the SIZ. The bimodal distribution remained recognizable even after averaging among all five animals (after normalizing each to their highest distance value, Figure 7J). Density values found on the greatest distance values most likely include the dendrites forming an arch toward the soma. Some of these dendrites were even scored among the highest 7 sub-trees, pertaining to the 75 percent of all putative GABAergic inputs (Figure 7 C-E).

In summary, putative GABAergic input is not evenly distributed among the branches comprising most of the dendritic surface, but it is instead more concentrated on dendrites closest and farthest from the SIZ. Thus, the highest quantities of putative GABAergic input were found on lower order branches, whereas the highest densities were localized at higher order branches. In agreement with this finding, analysis of individual sub-trees revealed that putative GABAergic synapses were preferentially located at sub-trees branching off the distal part of the primary neurite, including the dendrites arching toward the soma. Interestingly, the center and posterior half of the MN5 dendritic tree was mostly devoid of sub-trees containing higher percentages of putative GABAergic synapses (yellow arrow in Figure 6 C-F).

### 3.2.3 COMPARISON BETWEEN nACHR AND RDL DISTRIBUTION PATTERNS

In conclusion, regions with lower quantities of putative cholinergic inputs seem to receive high amounts of putative GABAergic input. Conversely, regions with lower quantities of putative GABAergic input seem to receive higher amounts of putative cholinergic input. Similarly, although the overall putative nAChR and Rdl density remains relatively constant, sub-trees that branch off closer to the center of the dendritic tree receive much higher total quantities of putative cholinergic inputs and distinctly reduced quantities of putative GABAergic inputs. Furthermore, in the case of putative cholinergic synapses, 10 sub-trees contained most of the input (75 percent), and in the case of putative GABAergic synapses, most of the input was located on only 7 sub-trees. Despite the seemingly complementary targeting of putative cholinergic and GABAergic synapses, there was still considerable overlap found between the localization of putative cholinergic and GABAergic synapses. High densities for both putative cholinergic and GABAergic input were found on higher order branches. These results suggest that GABAergic input is more concentrated on fewer sub-trees and dendritic regions than seems to be the case for putative cholinergic synapses.

## 3.3 DEVELOPMENTAL CHANGES OF NATIVE D $\alpha$ 7 nACH RECEPTOR AND RDL RECEPTOR EXPRESSION PATTERN IN THE *DROSOPHILA* RENTRAL NERVE CORD

In chapter 3.2, the results on the distribution patterns of putative cholinergic and GABAergic synapses were discussed and analyzed. One major finding was the seemingly inverse allocation of putative cholinergic and GABAergic input on the MN5 dendritic tree. In this chapter, I address the question of whether the expression of nAChR and GABA<sub>A</sub>-R, mediating excitatory and inhibitory signal transmission appears at the same time during pupal development, or if the expression of one receptor precedes the other. To test for native expression of nACh receptors and Rdl-GABA<sub>A</sub> receptors, the *Drosophila* VNC was incubated with antibodies raised against the D $\alpha$ 7 subunit of the nAChR (Fayyazuddin *et al.*, 2006) or Rdl-type GABA<sub>A</sub>-R (Raghu *et al.*, 2007).

### 3.3.1 *D $\alpha$ 7* EXPRESSION PATTERNS DURING PUPAL DEVELOPMENT OF *DROSOPHILA MELANOGASTER*

Antibody staining against the *D $\alpha$ 7* subunit of the nAChR was double-labeled with C380-GFP, for orientation purposes in the VNC (see methods). During the third instar larva (last larval stage, L3), *D $\alpha$ 7* nAChR was expressed abundantly in various neuronal cell bodies and processes throughout the VNC and showed significant overlap with the C380-GFP expression pattern (Figure 8A). Similarly, strong and abundant expression of nAChR in cell bodies and the neuropil was observed in the first pupal stage, P1 (~2 hours after puparium formation (APF), Figure 8B). However, the level of *D $\alpha$ 7* nAChR expression in neuronal cell bodies and the neuropil was decreased in the second pupal stage (P2), but the C380-GFP signal remained strong (~4 hours APF, Figure 8C). In stage P3 (~6 hours APF), *D $\alpha$ 7* nAChR expression is barely visible. Additionally, C380-GFP expression is confined to only a few cells compared with previous stages (Figure 8D). Interestingly, almost no *D $\alpha$ 7* nAChR expression was detectable at stage P4 (~8 hours APF), and remained absent in early P5 (~12.5 hours APF, Figure 8E, F). However, in stage early-P5, C380-GFP expression was observed in an increasing number of neuronal soma and within the neuropil, including the MN5 (Figure 8F, white arrows). *D $\alpha$ 7* nAChR expression was clearly detectable in various somata and the neuropil in the middle and late stages of P5 (P5m ~15 hours, P5l ~18 hours after APF). In these stages, *D $\alpha$ 7* nAChR expression was also present in the now identifiable MN5 soma and dendritic field (Figure 8G, H white arrows). In all older pupal stages, from P5l to P14 (not all data are shown), a strong *D $\alpha$ 7* nAChR expression in the VNC and MN5 soma and dendritic field could be detected. The adult VNC was also strongly positive for *D $\alpha$ 7* nAChR, and it showed robust expression in the MN5 soma and dendritic field. In summary, initially strong and abundant *D $\alpha$ 7* nAChR expression remains from the last larval stage to the first pupal stage, but vanishes during early pupal development. However, the *Drosophila* VNC regains *D $\alpha$ 7* nAChR expression in pupal stage P5 and it remains strong and robust through all later pupal stages and the adult.

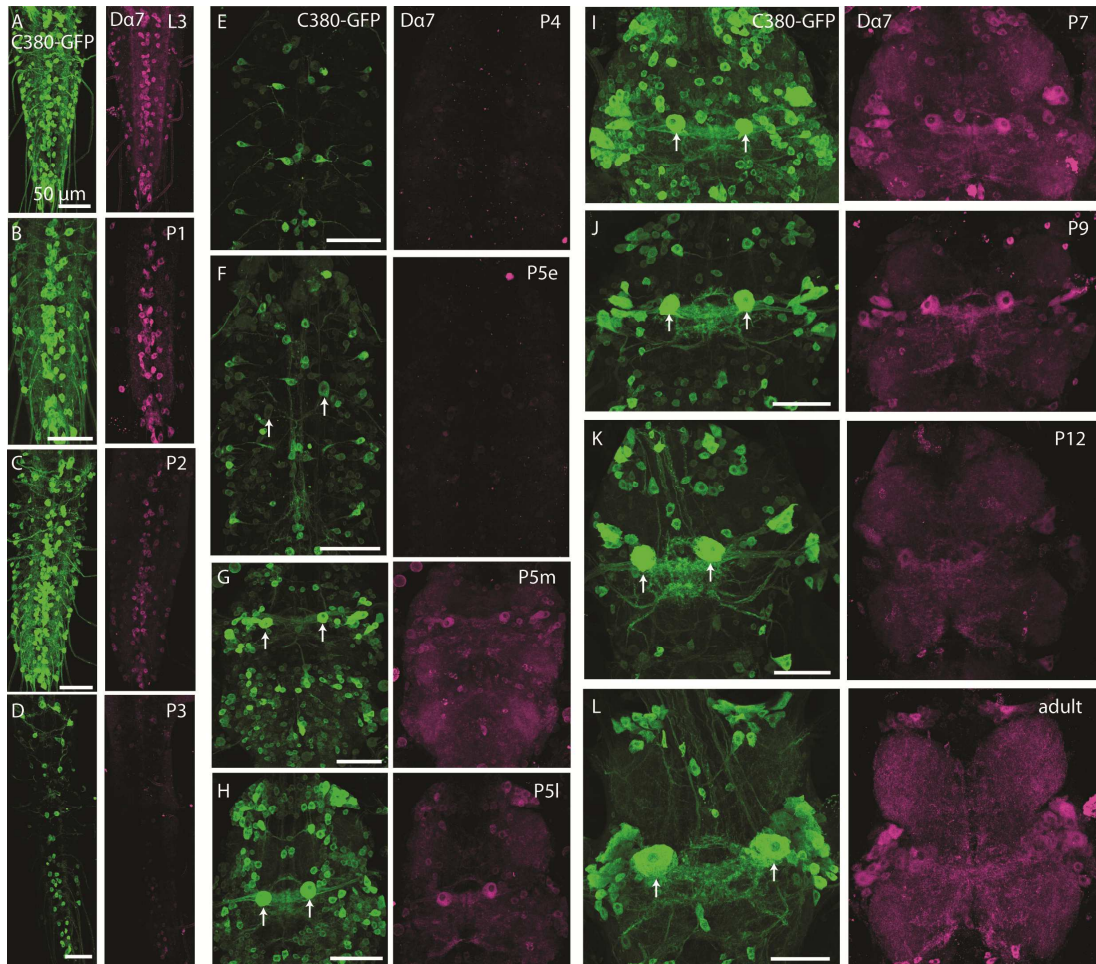


Figure 8: *Da7* Expression Patterns During Pupal Development of *Drosophila melanogaster*

The shown overview images are projections of all optical sections into one focal plane using the maximum intensity projection method to enable the viewer to get a comprehensive impression of the overall labeling pattern. Overviews of the thoracic ventral nerve cord following *Da7* nAChRs (right, magenta) and GFP immunocytochemistry in flies expressing UAS-mCD8-GFP under the control of C380-GAL4 (left, green) at different pupal stages.

(A) L3: third instar larvae. (B) P1: ~1 hour APF. (C) P2: ~3 hours APF. (D) P3: ~6 hours APF. (E) P4: ~8 hours APF. (F) early P5 (P5e): ~12.5 hours APF. (G) middle P5 (P5m): ~15 hours APF. (H) late P5 (P5l): ~18 hours APF. (I) P7: ~40 hours APF. (J) P9: ~58 hours APF. (K) P12: ~75 hours APF. (L) adult. White arrows point to MN5 somata at stages where it could be unambiguously identified by GFP expression. All scale bars: 50  $\mu$ m.

### *3.3.2 RDL EXPRESSION PATTERNS DURING PUPAL DEVELOPMENT OF DROSOPHILA MELANOGASTER*

Similar to the examination of nAChR expression patterns, various pupal stages were selected and the different patterns of native Rdl expression were documented (Figure 9). Rdl-antibody staining was again paired with C380-GAL4 driven GFP expression in neuronal membranes to reference the position of MN5. At the last larval stage (third instar larvae, L3), Rdl expression was found to be strongly present in the neuropil (Figure 9A). Expression was decreased in early pupal stage P2 (~3 hours APF, Figure 8B). In the following pupal stages, P3 (~6 hours APF), P4 (~8 hours APF), and early P5 (~12.5 hours APF), Rdl expression was barely detectable in the thoracic neuropil (Figure 9C, D, E). However, weak expression in the abdominal neuropil remained throughout these pupal stages (data not shown). During later stages of P5, weak Rdl expression was again detectable in the neuropil (Figure 9F). At stage P9 (~58 hours APF), a strong and abundant expression of Rdl in the neuropil was detected and remained through the adult stage (Figure 9G, H).

In summary, Rdl expression was strongly present in the last larval stage and started to decrease in early pupal developmental stage P2, which is similar to D $\alpha$ 7 nAChR expression pattern described above. In the following pupal stages, Rdl expression was barely detectable in the thoracic neuropil until pupal stage 5. Therefore, Rdl expression seems to reappear about the same time as nAChR, (i.e., during pupal stage 5 between ~12.5h and ~18h). However, the pattern for Rdl was more variable than for nAChR: In four sample preparations, the reappearance of Rdl expression ranged across the early, middle, and late P5 stages. However, all preparations revealed Rdl expression consistently at the later pupal stages of P5, about 18 hours APF, and it remained strong in all later developmental stages until the adult. Unfortunately, this study lacked the scope and resolution to effectively discern whether one of the receptors preceded the other when they reappeared during pupal development.

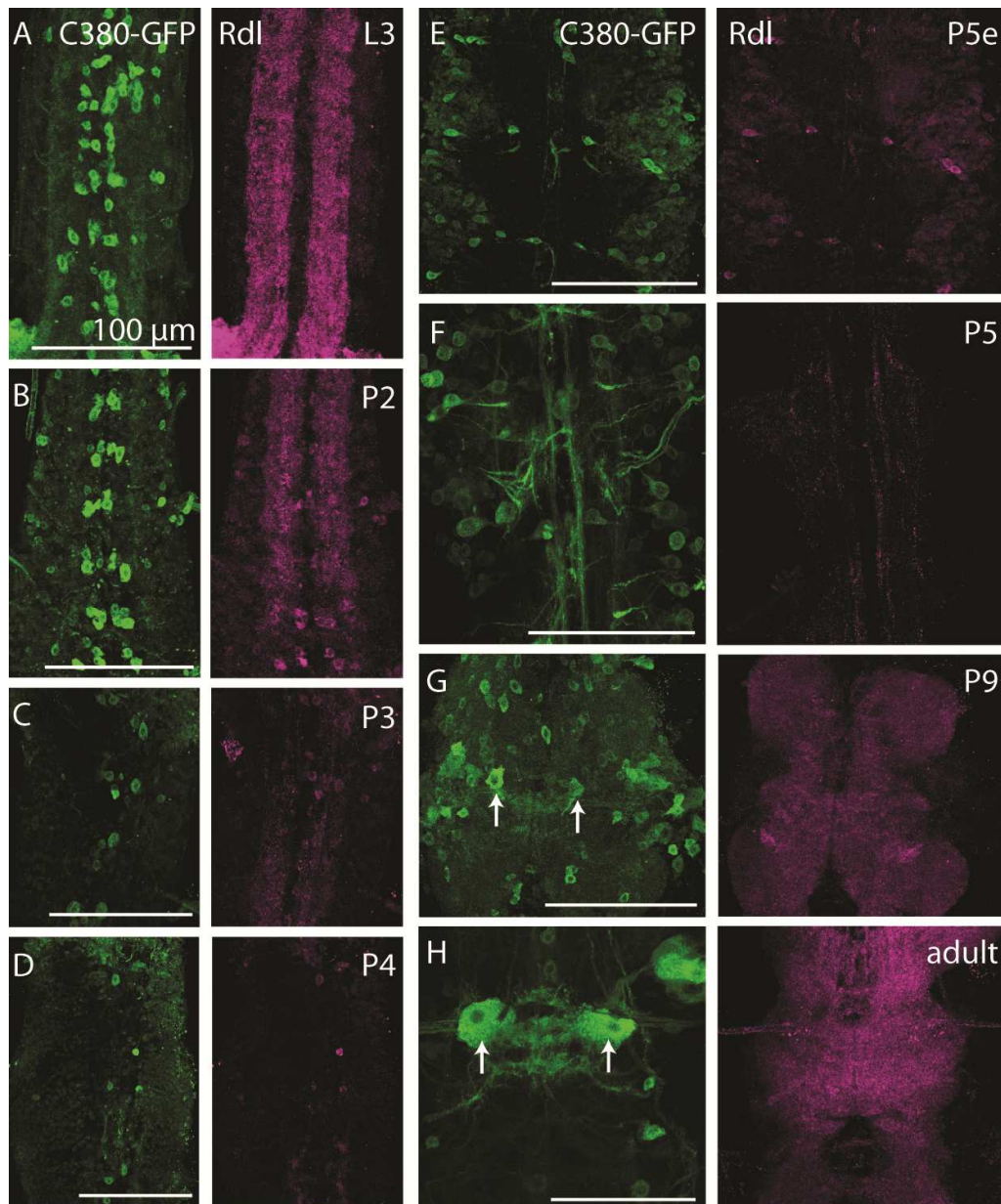


Figure9: *Rdl* Type GABA<sub>A</sub>-R Expression Patterns During Pupal Development of *Drosophila melanogaster*

The shown overview images are projections of all optical sections into one focal plane using the maximum intensity projection method to enable the viewer to get a comprehensive impression of the overall labeling pattern. Overviews of the thoracic ventral nerve cord following *Rdl* (right, magenta) and GFP immunocytochemistry in flies expressing UAS-mCD8-GFP under the control of C380-GAL4 (left, green) at different pupal stages.

(A) L3: third instar larvae. (B) P2: ~3 hours APF. (C) P3: ~6 hours APF. (D) P4: ~8 hours APF. (E) early P5 (P5e): ~12.5 hours APF. (F) P5: about 15~18 hours APF. (G) P9: ~58 hours APF. (H) adult. White arrows point to MN5 somata at stages where it could be unambiguously identified by GFP expression. All scale bars: 100  $\mu$ m.

### 3.3.3 DEVELOPMENT OF THE MN5 DENDRITIC TREE

The pupal development of the MN5 has been studied and described extensively by Consoulas *et al.* (2002). However, in order to relate the above findings (see chapters 3.3.1 and 3.3.2) to the model neuron MN5, four intracellular stainings, each depicting a representative stage of dendrite development, were prepared for this study (Figure 10). Similar to Consoulas *et al.* (2002), dendrite formation was found to begin in pupal stage P5. Only a few and very short dendritic branches are visible at first. A multitude of filopodia was originating from these short stump-like branches. Interestingly, in stage P6 these filopodia span across an area that seems to be the same region that would later be occupied by the adult dendritic tree of MN5. Unfortunately, these long and fragile filopodia collapsed during the fixation process. In pupal stage P7, multiple stable dendritic branches have been formed. At stage P11 of pupal development, the dendritic tree appears to already possess a complexity comparable to the adult. In summary, the onset of dendritic growth seems to occur at similar developmental stages as the expression of nAChRs and Rdl receptors.

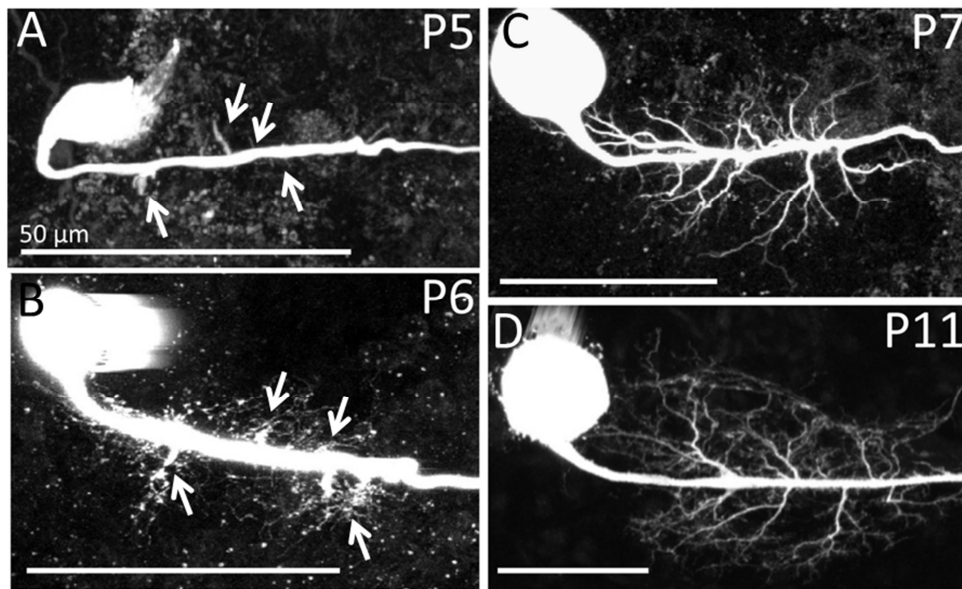


Figure 10: *Development of the MN5 dendritic tree*

Projection views of MN5 intracellular staining at different pupal stages.

A) P5: ~12.5-18 hours APF. (B) P6: ~25 hours APF. (C) P7: ~40 hours APF. (D) P11: ~70 hours APF. White arrows indicate first growing dendritic branches. In both (A) and (B) multiple filopodia are branching off the initial branches, which collapsed and were not visible in (A) anymore after fixation. For a more detailed description of MN5 dendritic outgrowth see Consoulas *et al.* (2002).

## 4 DISCUSSION

This study identified the putative location of the spike initiating zone (SIZ) at the distal region of the primary neurite in the *Drosophila* flight motor neuron MN5. By exploiting the conserved morphology of identified dendritic sub-trees in different animals (Vonhoff & Duch, 2010), a method was developed to predict the SIZ with 70 percent accuracy in MN5 preparations without additional sodium channel immunocytochemistry. This newly developed technique was then applied to analyze putative cholinergic and GABAergic input onto the MN5 dendritic tree with regard to the SIZ. The results indicate that putative excitatory and inhibitory synapse distributions localize mostly in inverse dendritic domains. Lastly, native nAChR and Rdl type GABA<sub>A</sub> receptor distributions were documented during pupal development of *Drosophila*. The key findings and their implications for MN5 function are discussed below.

### 4.1 ESTIMATING THE LOCATION OF THE SPIKE INITIATING ZONE IN MN5

The identification of where information enters the neuron and where it is being converted into an output signal is essential in the process of understanding neuronal communication. It is known that action potentials are generated in the axon of a neuron and require high densities of voltage gated sodium and potassium channels. In vertebrate neurons the axon initial segment (AIS), which separates the neuron's somatodendritic region from its axonal domain, has been identified as the most likely location for action potential initiation (Palmer & Stuart, 2006). With 40-50 times higher densities for VGSC, the AIS facilitates a high sodium current density and a low threshold for action potential generation (Kole *et al.*, 2008; Lorincz & Nusser, 2010; Kole & Stuart, 2008). During the last decade, multiple studies have identified various intrinsic and extrinsic mechanisms to be responsible for ion-channel placement and maintenance within the AIS. Many of the involved molecules are also key players in the generation of neuronal polarity, neurite compartmentalization, and trafficking (reviewed in Katsuki *et al.*, 2011; Horton & Ehlers, 2003). The scaffolding molecule Ankyrin G has been recognized as the major organizing

protein at the AIS of vertebrate neurons. It is responsible for tethering membrane proteins and ion-channels, for instance VGSC, to the cytoskeleton. Loss of Ankyrin G results in the loss of sodium and potassium channel clustering at the AIS (Zhou *et al.*, 1998; Hedstrom *et al.*, 2007; Pan *et al.*, 2006; Van Wart *et al.*, 2007). Ankyrin G consequently establishes subcellular polarity of various molecules (Rasband, 2010). Taken together, an enrichment of voltage-gated sodium and potassium channels and Ankyrin G are essential for the definition of the AIS in vertebrate neurons. However, the anchor motif in sodium and potassium channels that facilitates their attachment to Ankyrin G, and hence the clustering of ion channels in the AIS, did not evolve before the appearance of early chordates and is therefore missing in invertebrates like *Drosophila* (Hill *et al.*, 2008). Nevertheless, recent studies show that *Drosophila* does have an AIS-like domain located at the proximal axonal segment (Rolls *et al.*, 2007; Trunova *et al.*, 2011). The putative *Drosophila* AIS has been characterized by the lack of somatodendritic and axonal markers, a unique actin organization, the accumulation of an ankyrin isoform, Ankyrin1, and specific targeting of voltage-gated potassium channels (Rolls *et al.*, 2007; Trunova *et al.*, 2011). Similar to the Kv1 localization at the AIS in vertebrate neurons (Duflocq *et al.*, 2011), *Drosophila* Shaker channels (Kv1-like A-type potassium currents) concentrate on the MN5 axon and, presumably, the axonal membrane (Ryglewski & Duch, 2008). Although Shaker immunocytochemistry was also detectable in the MN5 soma, the primary neurite, from which all the dendrites branch off, was only weakly positive for Shaker. Therefore, Ryglewski & Duch (2008) suggest targeted transport of Shaker from the soma to the axonal segment of MN5. Mapping these potassium channels onto a MN5 surface reconstruction showed an increase in staining intensity beginning at the most distal region of the MN5 primary neurite and beyond in throughout the axon (Ryglewski & Duch, 2008).

Previously, Duch *et al.* (2008) demonstrated that action potentials in MN5 are mediated by TTX sensitive fast sodium channels. It was therefore assumed that action potential propagation requires high densities of TTX sensitive fast sodium channels in the axonal membrane of MN5. In this study, the localization of such voltage-gated sodium channels (VGSC) was used to estimate the spike initiation zone in MN5. The specificity of the VGSC antibody SP19 for insect nervous tissue was shown in several previous studies (French *et al.* 1993; Amat *et al.* 1998; Boerner *et al.* 2006) and in this study by Western Blotting. Indeed, VGSC positive label was found in consistently high densities throughout the whole MN5 axon. Furthermore, VGSC label seemed to be located predominantly in the

membrane of the axon. However, the optical resolution (120 nm x 120 nm x 300 nm) of confocal images is not sufficient to definitively argue for VGSC localization in the membrane. Additionally, VGSC labeling was only faint in the majority of the primary neurite, which connects the soma with the axon, and from where most the dendrites are branching off. However, the faint staining increased significantly in the distal portion of the primary neurite (at  $88 \pm 15$   $\mu\text{m}$  from the soma), where only a few dendrites are branching off. This pattern, of faint VGSC in the proximal primary neurite and increased intensity in the distal segment of the primary neurite, mirrors the results found for Shaker potassium channel localization (Ryglewski & Duch, 2009). It can therefore be proposed that the faint VGSC staining found in the proximal primary neurite, similar to the Shaker staining results from Ryglweski and Duch, indicates transport of sodium channel proteins to the distal portion of the primary neurite and axonal segment. Additionally, recordings from the soma of MN5 showed amplitude attenuation and broadening to a degree that suggests their initiation at about 100  $\mu\text{m}$  from the soma (Duch *et al.*, 2008), and this data places the SIZ at about the same distance from the soma where a sharp increase in sodium channel staining intensity was found in this study. Taken together, these findings strongly suggest that VGSC immunocytochemistry is an appropriate tool to locate the putative spike initiating zone in MN5. Moreover, this study indicates that voltage-gated potassium and sodium channel presumably co-localize at the putative *Drosophila* SIZ, as they do at the vertebrate AIS. However, further investigations are needed to confirm that the location of the proposed SIZ matches with the localization of other cell polarity molecules. A recent study in *Drosophila* mushroom body neurons proposed Cdk5/p35 kinase in the recruitment of Ankyrin1 to the potential axonal segment (Turnova *et al.*, 2011), which would be a good candidate for these further investigations.

## 4.2 SPATIAL SEPARATION OF PUTATIVE CHOLINERGIC AND GABAERGIC SYNAPSES TO DIFFERENT DENDRITIC REGIONS

This study examined the dendritic distribution of  $\text{D}\alpha 7$  nAChR and Rdl type  $\text{GABA}_A$ -Rs in the motor neuron 5 of the adult *Drosophila* fly. The location of synaptic input on a complex dendritic tree with respect to the SIZ, as well as the relative position of excitatory and inhibitory synapses to each other, has been shown to influence dendritic computation and firing output in many neurons (reviewed in: London & Haeusser, 2005;

Koch and Segev, 2000; Haeusser & Mel, 2003). Therefore, I first estimated the SIZ in MN5 reconstructions and then analyzed putative GABAergic and cholinergic input locations with respect to the SIZ.

The findings of this study show that putative cholinergic and GABAergic synapses are mostly spatially separated and seem to occupy inverse dendritic domains of the MN5 dendritic tree. The majority of putative cholinergic input was distributed widely at low densities on sub-trees proximal to the soma, whereas putative GABAergic synapses were found to be concentrated on sub-trees branching off the SIZ at the distal segment of the primary neurite. Furthermore, highest quantities of putative cholinergic input were found on intermediate branch orders and distances. In contrast, the highest quantities for GABAergic input were located on lower branch orders and distances closer to the SIZ. However, the highest densities for both receptor types were located on the higher order branches.

The findings in this study differ from distributions found in other invertebrate neurons. In *Manduca*, GABAergic synapses were found to localize predominantly at distal dendrites in the adult MN5 dendritic tree (Meseke *et al.*, 2009). In lobula plate tangential neurons of the fly, both excitatory and inhibitory inputs are targeted to distal dendrites (Raghu *et al.*, 2007; 2009). The different localization patterns for excitatory and inhibitory synapses in these different neurons suggest different requirements for synaptic placement and signal integration. Meseke *et al.* (2009) hypothesized that the developmental change in distribution pattern for GABAergic synapses, from a randomized distribution in the larva to a more focused localization on distal dendrites in the adult MN5, may reflect changes from a slow larval crawling neuron to a fast adult flight motor neuron. Likewise, co-localization of excitatory and inhibitory synapses onto distal dendrites in lobula plate tangential neurons has been hypothesized to aid visual motion processing (Raghu *et al.*, 2007). Therefore, both studies strongly suggest dendritic polarity and targeting of synapses to distinct dendritic locations as conserved mechanisms to control dendritic computation. This study also demonstrated preferred targeting of excitatory and inhibitory input to spatially separated dendritic domains in the *Drosophila* flight motor neuron MN5. Furthermore, the concentration of cholinergic and GABAergic input at higher order branches could also indicate distinct molecular identities for individual dendritic segments (Horton & Ehler, 2003). However, contrary to lobula plate tangential cells, the findings of this study suggest predominantly domain specific computation of information, rather than

local integration. Such domain-specific computation has been suggested for pyramidal neurons (Pouille & Scanziani, 2001). Pyramidal neurons are one of the best studied vertebrate neurons with complex dendritic trees. Interestingly, the distribution patterns for excitatory and inhibitory input found for MN5 show resemblance with the patterns described for pyramidal CA1 neurons. In pyramidal neurons, excitatory input has been shown to localize predominantly on distal dendrites, whereas inhibitory input is mainly targeted to the perisomatic region, soma and AIS (Megias *et al.*, 2001). Based on this spatially separated distribution pattern, a non-selective inhibitory veto function has been suggested to control neuron output patterns and to synchronize neuronal activity among pyramidal neurons (Megias *et al.*, 2001; Di Cristo *et al.*, 2004). How these distribution patterns may be aiding the neuron's dendritic computational requirements will be discussed in the paragraphs below.

MN5 is one out of five motor neurons innervating the 6 muscle fibers of the DLM (Cogshall, 1978, Koenig & Ikeda 1980a; b). The DLM is a large stretch-activated asynchronous power muscle that is responsible for the downstroke of the *Drosophila* wing (Machin & Pringle, 1959). Extracellular recordings of MN1-5 during restrained flight have shown that the firing frequencies increase and decrease simultaneously and slowly (Dickinson & Tu, 1997; Levine & Wyman 1973; Harcombe & Wyman 1977). More recent research revealed that the changes in motoneuron firing frequencies correlate linearly with intramuscular calcium concentrations, which in turn correlate linearly with changes in wing beat frequency and power output during normal restrained flight (Gordon & Dickinson, 2006). Although all 5 motor neurons fire tonically and in a characteristic sequential pattern, they do not fire at the same time (Koenig & Ikeda, 1980a; b; Levine & Wyman, 1973; Harcombe & Wyman, 1977). Based on extra- and intracellular recordings, Koenig & Ikeda (1980a; 83) proposed an excitatory effect and weak electronic coupling as cause for the characteristic firing frequencies found in these motor neurons. Levine & Wyman (1973), however, suggested a system of mutual inhibition. Based on their extracellular recordings, they predicted that the characteristic firing patterns of the motor neurons innervating the DLM are achieved via both, a common excitatory drive and inhibitory connections between the motor neurons (Harcombe & Wyman 1977). The results from this study utilizing immunocytochemistry and high resolution confocal microscopy seem to support the latter hypothesis.

Steady tonic firing, as described for the *Drosophila* motor neurons innervating the DLM, and slow adjustments in response to increased excitatory drive can be achieved by the summation of many EPSPs (London & Haeusser, 2005; Koch and Segev, 2000; Haeusser & Mel, 2003). This is consistent with the distribution pattern of putative cholinergic synapses found in this study. High quantities of putative nAChRs that are spread out over many dendritic branches and sub-trees, and which are relatively distant to the SIZ, could provide the excitatory input necessary to elicit tonic firing. Additionally, concentrated inhibitory input at the SIZ, as found in this study, may enable the sharp inhibition needed to provide the inhibitory control proposed by Harcombe and Wyman (1973). Such focused inhibition close to the SIZ would not influence tonic firing frequencies but ensure preferred sequential firing of MN1-5 during flight. Furthermore, the exceptionally long dendrites, which originate at the SIZ and grow backward towards the soma, show high densities for Rdl, but not nAChR. An attractive hypothesis would be that these long dendrites, which possess most of their branches at the very end, collect additional inhibitory drive from that region of the neuropil and direct it to the SIZ. Taken together, the spatial distribution of excitatory and inhibitory input found in this study match the predictions derived from simultaneous extra cellular recordings of MN1-5 (Levine & Wyman 1973; Harcombe & Wyman 1977). Therefore, the distribution patterns revealed in this study are in agreement with the data available for the function of synaptic drive in *Drosophila* flight motor neurons during restrained flight. However, this study also showed high densities for both nAChRs and GABA<sub>A</sub>-Rs on higher order branches. Concentrated inhibitory and excitatory synapses on the same dendritic branches can be indicative of local computation. High densities of cholinergic synapses could lead to sub-linear summation if they are activated simultaneously. Likewise, co-localization of inhibitory and cholinergic synapses on the same dendritic branches could cause shunting inhibition if they were activated at the same time. Consequently, the distributions found for nAChRs and GABA<sub>A</sub>-Rs suggest both local dendritic computation on higher order branches and domain-specific computation with a non-selective inhibitory veto function for most inputs of the dendritic tree.

Recent findings in our laboratory and other studies (Ryglewski unpublished data; Kadas *et al.*, 2012) have shown that MN5 can fire at much higher frequencies than those reported for experiments conducted under restrained flight conditions. During restrained flight, flies do not have to carry their own weight. Under these circumstances MN5 fires at a frequency at about 10-20 Hz (Harcomb & Wyman, 1973). In contrast, current

injection performed by S. Ryglewski and presynaptic stimulation performed by Kadas *et al.* (2012) show frequencies ten times as high. Recent research on pyramidal neurons suggests that these neurons are able to perform two types of dendritic integration depending on the behavior state requirements. Depending on the timing of input onto the dendritic tree, excitatory input is either sub-threshold, and is integrated linearly based on dendritic architectural features, or excitatory input is received simultaneously, and based on active dendritic properties leads to non-linear integration of input signals (Gasparini & Magee, 2006). As mentioned above, most data on *Drosophila* flight motor neuron firing was collected during restrained flight experiments, in which the animals do not carry their own weight and maximal output-power might not be necessary. However, to attain these high firing frequencies, normal excitatory drive might require boosting. Similar to pyramidal neurons, active dendritic properties could be activated in concert with temporal coordinated excitatory input. The presence of high voltage-gated calcium channels Cav1 and Cav3 have been previously reported in MN5 (Ryglewski *et al.*, 2012). The signal from excitatory drive to dendritic domains more distant to the SIZ could be further enhanced via these calcium channels and potentially lead to increases in firing frequency of MN5, as well as increased wing beat frequency and power output of the DLM. Simultaneous activation of clustered nAChRs on distal sub-trees and higher order branches could lead to voltage changes significant enough to open these calcium channels during high power demand situations. However, predictions about possible computational processes remain speculative without more detailed experiments, for instance, the investigation of input timing and synaptic strength. Additionally, the data derived from this study's reconstructions, distribution maps, and the location of the putative SIZ can be exported into the NEURON modeling environment (Hines & Carneval, 1997; 2001) to test predictions about possible functions of synaptic distribution in multi-compartment models (Ryglewski & Duch, 2009; Meseke *et al.*, 2009).

### 4.3 CRITICAL ANALYSIS OF THE METHOD USED FOR MAPPING PUTATIVE SYNAPTIC INPUTS TO MN5 DENDRITES

In this study, tagged receptors were expressed under the control of non-native promoters to examine the distribution of cholinergic and GABAergic inputs via confocal microscopy. Receptor locations documented by confocal microscopy were then mapped

onto MN5 surface reconstructions. Although this is an accepted method and has been proven as a useful practice in *Drosophila* in former studies, this process bears problems.

First, the optical resolution of confocal microscopy is below the size of synapses. Only electron microscopy (EM) provides error free mapping of synapses to central neurons (Briggman & Denk, 2006). Recent technological advances have developed EM into a more efficient and suitable method for synapse localization. However, even advanced block face scanning EM is extremely time consuming compared to confocal microscopy, and it requires special expensive equipment. Localizing synapses with confocal microscopy onto dendritic surface reconstructions has been evaluated by EM technique, and it was shown that if postsynaptic and presynaptic markers are used in conjunction, all synapses were accounted for and false positives can be reduced to less than 20 percent (Hohensee *et al.*, 2008). Therefore, positively scored input sites on MN5 surface reconstructions can only be seen as candidates for cholinergic and GABAergic input sites. Further, locations devoid of positive label can be assumed not to represent input sites. This method consequently does not provide any information about synaptic strength or the exact size of synapses. Therefore, this method only provides an estimate of where cholinergic and GABAergic input sites are predominantly located and whether they do or do not co-localize to specific dendritic sub-domains.

Second, expression of tagged receptor subunits under the control of non-native promoters bears the problem of potentially mis-targeting these receptor subunits. However, because only the expression of subunits (D $\alpha$ 7, Rdl) is under the control of non-native promoters, the other subunits should be expressed and targeted normally. Therefore, it can be assumed that effects on the localization of fully resembled receptors are limited. Although both constructs used have been already carefully studied, and were successfully used in localization studies in *Drosophila* (Raghu *et al.*, 2007; 2009; Fayyazuddin *et al.*, 2006.), such mis-targeting cannot be excluded. While careful comparison between receptor expression pattern and native-antibody staining did not reveal any obvious differences, and both staining methods showed punctuated patterns co-localized with presynaptic markers, only rigorous quantification can rule out any potential for mis-targeted expression.

Third, in the scope of this study only D $\alpha$ 7 nAChR and Rdl type GABA $_A$ -R have been considered and were discussed in the light of previous studies. However, it cannot be excluded that other excitatory and inhibitory input receptors are present and might affect

the firing behavior of MN5. Nevertheless,  $D\alpha 7$  is the predominant excitatory receptor type in the *Drosophila* escape circuitry, which includes MN1-5 (Fayyazudin *et al.*, 2006). Similarly, RDL is the most abundantly expressed GABA<sub>A</sub>-R in *Drosophila* central neurons (Harrison *et al.*, 1996; Liu *et al.*, 2007; Agosto *et al.*, 2008; Raghu *et al.*, 2007). Therefore, most inhibitory and excitatory input should be mediated by these two types of receptors.

Consequently, I am confident that within the limits of this method a valid estimate about the distribution pattern of excitatory and inhibitory input synapses to MN5 dendrites is possible. Furthermore, this method has been used with great success in previous studies, and it has yielded valuable data about synapse localization in *Manduca* (Duch & Mentel, 2004; Meseke *et al.*, 2009) and *Drosophila* neurons (Raghu *et al.*, 2007; 2009).

#### 4.4 NICOTINIC ACh AND GABA<sub>A</sub> RECEPTOR EXPRESSION PATTERNS DURING *DROSOPHILA* PUPAL DEVELOPMENT

Antibody staining against the natively expressed nAChR and GABA<sub>A</sub>-R revealed that these two types of receptors followed a similar time course of expression during postembryonic development of *Drosophila*. Interestingly, both receptor expressions disappeared at the early pupal stages P2-3 and reappeared during pupal stage P5. Intracellular stainings of MN5 at stages P5 to P11 showed that the reappearance of both receptors correlate with the initial outgrowth of MN5 dendrites and filopodia extensions.

A multitude of studies in vertebrates and invertebrates have investigated the complex mechanisms underlying dendritic growth and synaptogenesis (reviewed in: Katz & Shatz, 1996; Wong & Gosh, 2002; Redmond & Gosh, 2005; Cline & Haas, 2008). Although many of the complex pathways involved are still not well understood, these studies indicate that activity-dependent influx of calcium plays a key role in dendrite formation and the maturation of synapses. Neurotransmitters, as mediators of neuronal activity, are well suited to bridge pre- and postsynaptic signaling events, and they may also influence developmental events prior to synapse formation (Nguyen *et al.*, 2001; LoTurco *et al.*, 1995). In vertebrates, initial calcium influx is facilitated by glutamate acting on AMPA receptors, which mediate most of the fast excitatory transmission in the brain and are initially highly permeable for calcium (Eybalin *et al.*, 2004; Miguez *et al.*, 2007). Therefore,

glutamate receptors have been intensively studied in the past, and they are implicated in the regulation of synapse formation, maturation, plasticity, and the development of dendritic and axonal arbors (Redmond & Gosh, 2005; Cline & Haas, 2009). The role of GABA acting on inhibitory GABA<sub>A</sub>-R in neuronal growth processes has been studied to a much lesser extent. Although GABA was initially discovered as an inhibitory transmitter, its role during developmental processes has been largely explained by its depolarizing action in immature neurons (Owens & Kriegstein, 2002; Ben-Ari *et al.*, 2007; Leinekugel *et al.*, 1995; LoTurco *et al.*, 1995). Therefore, both glutamate and GABA are depolarizing the membrane of immature vertebrate neurons, which can lead to calcium influx through voltage-gated calcium channels (LoTurco *et al.*, 1995), and this can initiate activity-dependent pathways involving CaMKs, CREB, and Crest (reviewed in Flavell & Greenberg, 2008).

In *Drosophila*, nAChRs mediate fast excitatory transmission, and they are known to be permeable for calcium (Leech & Satelle, 1993; Oliveira *et al.*, 2010). They are therefore an attractive candidate for activity-dependent regulation of dendritic growth and synaptic maturation in *Drosophila*. This study could show that, during metamorphosis and neuron remodeling in *Drosophila*, the reappearance of nAChR expression correlates with the onset of initial dendritic growth in MN5. However, at this point and without further study, the effects of nAChR mediated calcium influx on dendrite development or synapse maturation remain speculative. For instance, it is not known if MN5 calcium influx is solely mediated by nAChR on early dendrites or if calcium channels are the main carrier for calcium ions in early developmental stages of MN5. Further, Chang and Berg (2001) showed that, in case of combined calcium influx via ion channels and nAChRs, L-type voltage-gated calcium channels block the effects of nicotinic signaling on transcription in vertebrate neurons. However, a recent study on embryonic motor neurons (aCC) in *Drosophila* supports the premise of locally controlled dendritic growth through cholinergic activity (Tripodi *et al.*, 2008). The morphometric changes of aCC forming dendrites in response to cholinergic activity were thought to be mediated by PKA in the motor neuron. Therefore, Tripodi *et al.* (2008) propose a key role for synaptic activity in the plastic arrangement of dendrites and synapses early in development, and as a mechanism to ensure a proper level of input.

In addition, Rdl type GABA receptors in *Drosophila* mediate fast inhibitory transmission (Harrison *et al.*, 1996; Liu *et al.*, 2007, Agosto *et al.*, 2008, Raghu *et al.*,

2007). Blocking GABA<sub>A</sub>-R by PTX bath application was shown to increase spontaneous firing in *Drosophila* neuronal cell culture and increase dendritic growth in developing *Manduca* motor neurons (Lee *et al.*, 2003; Meseke *et al.*, 2009). Furthermore, genetic deletions removing the glutamic acid decarboxylase locus or the Rdl type GABA receptor locus resulted in embryonic lethality (Kulkarni *et al.*, 1994; Stilwell *et al.*, 1995). This indicates an important role of the GABAergic system in early neural development of *Drosophila*. The reported expression patterns of Rdl type GABA<sub>A</sub>-R, and their reappearance concurrent with the beginnings of MN5 dendritic growth, further strengthen the role of GABA<sub>A</sub>-Rs during early neuronal development similar to that in vertebrates.

The formation of mature distribution patterns of inhibitory synapses in MN5 of *Manduca* and pyramidal neurons in vertebrates, (Meseke *et al.*, 2009; Di Cristo *et al.*, 2004) are thought to be mostly independent of activity and primarily genetically pre-determined. On the other hand, experience guided sub-cellular synapse elimination was found to confine inhibitory glycinergic input in auditory interneurons in rodents (Kapfer *et al.*, 2002). At this point, it remains unclear, which mechanisms act in the placement of synapses in the MN5 of *Drosophila*. However, inhibitory and excitatory terminal distributions in the neuropil of *Drosophila* have been previously investigated. Higher concentrations of GABAergic terminals and cholinergic terminals were found in the depressor flight motoneuron neuropil (Boerner & Duch, 2010). Likewise, this study could show increased GABA<sub>A</sub>-Rs densities in MN5 dendritic areas. Although the neuropil of both, *Drosophila* and *Manduca* appears non-layered, the increased densities of GABAergic and cholinergic terminals are in contrast with the even distribution found in the flight motoneuron neuropil of *Manduca* (Meseke *et al.*, 2009). Concentrated GABAergic and cholinergic input, together with regionally concentrated GABA<sub>A</sub>-Rs, could hint toward presynaptically guided and activity dependent mechanisms for the placement of synapses in the *Drosophila* MN5. Extrinsic signals, for instance secreted semaphorins (Polleux *et al.*, 2000) and neurotrophins (Huang & Reichardt, 2003), have been suggested to be involved in the targeting receptors to specific dendritic sub-domains and segments (Horton & Ehlers, 2003). However, whether the targeting of receptors and the placement of synapses in the MN5 of *Drosophila* solely depends on activity and pre-synaptic guidance, or if pre-determined targeting mechanisms also play a role, as proposed for the MN5 in *Manduca* and pyramidal neurons, remains to be determined.

## 5 ABSTRACT

For efficient synaptic transmission, postsynaptic neuronal receptors need to be localized in precise apposition to presynaptic terminals that release the neurotransmitter. Modeling and electrophysiological studies have shown that the location of input synapses in complex dendritic trees can affect the computational properties of the postsynaptic neuron. First, this study defined the putative location of the spike initiating zone (SIZ) at the distal region of the primary neurite in the *Drosophila* flight motor neuron MN5. By exploiting the conserved morphology of identified dendritic sub-trees in different animals, a method was developed to predict the SIZ with 70 percent accuracy in MN5 preparations without sodium channel immunocytochemistry. This technique was then applied to investigate whether sub-dendritic targeting and clustering occurs in a transmitter specific manner in complex dendritic trees of the identified flight motor neuron MN5, located in a non-layered neuropil in *Drosophila melanogaster*. Nicotinic acetylcholine receptors containing  $\text{D}\alpha 7$  subunits mediate fast excitatory signaling at most synapses in the *Drosophila* escape circuit, including synapses to MN5. The most abundant fast inhibitory receptors in insect central neurons are ionotropic  $\text{GABA}_A$  receptors. Immunocytochemistry and targeted expression of tagged receptors was used to map the expression of the Rdl subunit of the  $\text{GABA}_A$ -R and the  $\text{D}\alpha 7$  subunit of the nicotinic AChR onto three-dimensional geometric reconstructions of MN5. The results indicate that putative excitatory and inhibitory synapse distributions localize mostly in inverse dendritic domains. Previous studies have predicted that during flight MN5 integrates tonic excitatory cholinergic drive into steady firing frequencies, and that those specific sequences of motor neuron firing are ensured by sharp inhibitory feedback within the central pattern generating network. Finally, native nAChR and Rdl type  $\text{GABA}_A$  receptor distributions were documented during pupal development of *Drosophila*. Interestingly, the onset of dendritic growth seems to correlate with the expression-onset of nAChRs and Rdl receptors in the early pupal stages during *Drosophila* metamorphosis. These results support a proposed role for synaptic activity mediated by nAChR and  $\text{GABA}_A$ -R in the development and growth of dendrites and synaptogenesis in *Drosophila* motor neurons.

## 6 ZUSAMMENFASSUNG

Für die effiziente Weiterleitung von synaptischen Potenzialen ist es von Nöten, dass postsynaptische Rezeptoren präzise ihren präsynaptischen Terminalen gegenüber liegen. Modelling und elektrophysiologische Studien haben gezeigt, dass die Position von Eingangssynapsen in komplexen dendritischen Bäumen die Signalverarbeitung in postsynaptischen Neuronen stark beeinflusst. Im Zuge dieser Arbeit wurde zuerst die Position der Aktionspotenzialgenerierung (APG) untersucht. Die Ergebnisse zeigten, dass Aktionspotenziale im motor neuron 5 (MN5) von *Drosophila* höchstwahrscheinlich in der distalen Region des primären Neuriten generiert werden. Basierend auf der konservierten Morphologie der dendritischen Unterbäume in MN5, konnte mit 70-prozentiger Wahrscheinlichkeit die Position der APG auch in anderen MN5-Präparationen ohne zusätzliche Natrium-Antikörper-Färbung geschätzt werden. Unter Zuhilfenahme dieser Schätzung wurden die relativen Positionen von Eingangssynapsen zur Position der APG untersucht. Die Fragestellung war, ob in dem komplexen dendritischen Baum von MN5 sich die Synapsen von verschiedenen Transmitter-Klassen in unterschiedlichen dendritischen Regionen konzentrieren. Nikotinischer Acetylcholin-Rezeptor (nAChR) mit der  $\text{D}\alpha 7$ -Untereinheit ist für die Weiterleitung schneller exzitatorischer Signale im MN5 und in anderen Neuronen des *Drosophila*-Flucht-Reflexes-Kreislaufes verantwortlich. Der meistverbreitete Rezeptor, verantwortlich für die Weiterleitung schneller inhibitorischer Signale, ist der ionotropische  $\text{GABA}_A$ -Rezeptor mit der Untereinheit Rdl. Die Verteilungsmuster der nAChR und  $\text{GABA}_A$ -Rezeptoren auf MN5-Dendriten wurden unter Zuhilfenahme von gezielter Expression der Rdl- und  $\text{D}\alpha 7$ -Untereinheit im MN5 und Immunocytochemie dokumentiert und dann auf dreidimensionale Rekonstruktionen der MN5 Oberfläche projiziert. Die gefundenen Verteilungsmuster für nAChR und  $\text{GABA}_A$ -R zeigten, dass sich die Rezeptoren in verschiedenen dendritischen Regionen konzentrieren. Vorherige Studien haben spekuliert, dass tonisches Feuerverhalten von MN5 während des Fluges mit inhibitorischem Eingang moduliert und präzisiert wird. Die Verteilungsmuster von nAChR und  $\text{GABA}_A$ -R unterstützen diese Vermutung. Des Weiteren wurden in dieser Arbeit die Verteilungsmuster von nAChR und  $\text{GABA}_A$ -Rs während der Puppenentwicklung von *Drosophila* dokumentiert und in Verbindung mit der dendritischen Entwicklung von MN5 interpretiert. Interessanterweise fällt das Erscheinen von beiden Rezeptorklassen mit dem

ersten Auswachsen von Dendriten in MN5 zusammen. Daher untermauern diese Daten die Rolle von synaptischer Aktivität bei der Entwicklung von Dendriten und Synapsen.

## 7 REFERENCES

- Aberle, H., Haghighi, A.P., Fetter, R.D., McCabe, B.D., Magalhaes, T.R. & Goodman, C.S. (2002) wishful thinking encodes a BMP type II receptor that regulates synaptic growth in *Drosophila*. *Neuron*, **33**, 545-558.
- Agmon-Snir, H., Carr, C.E. & Rinzel, J. (1998) The role of dendrites in auditory coincidence detection. *Nature*, **393**, 268-272.
- Agosto, J., Choi, J.C., Parisky, K.M., Stilwell, G., Rosbash, M. & Griffith, L.C. (2008) Modulation of GABA(A) receptor desensitization uncouples sleep onset and maintenance in *Drosophila*. *Nature Neuroscience*, **11**, 354-359.
- Amat, C., Lapied, B., French, A.S. & Hue, B. (1998) Na<sup>+</sup>-dependent neuritic spikes initiate Ca<sup>2+</sup>-dependent somatic plateau action potentials in insect dorsal paired median neurons. *Journal of Neurophysiology*, **80**, 2718-2726.
- Andrasfalvy, B.K. & Magee, J.C. (2001) Distance-dependent increase in AMPA receptor number in the dendrites of adult hippocampal CA1 pyramidal neurons. *Journal of Neuroscience*, **21**, 9151-9159.
- Armstrong, D., Dunn, J.K., Antalffy, B. & Trivedi, R. (1995) SELECTIVE DENDRITIC ALTERATIONS IN THE CORTEX OF RETT-SYNDROME. *Journal of Neuropathology and Experimental Neurology*, **54**, 195-201.
- Barnard, E.A., Skolnick, P., Olsen, R.W., Mohler, H., Sieghart, W., Biggio, G., Braestrup, C., Bateson, A.N. & Langer, S.Z. (1998) International Union of Pharmacology. XV. Subtypes of gamma-aminobutyric acid(A) receptors: Classification on the basis of subunit structure and receptor function. *Pharmacological Reviews*, **50**, 291-313.
- Bellen, H.J., Okane, C.J., Wilson, C., Grossniklaus, U., Pearson, R.K. & Gehring, W.J. (1989) P-ELEMENT-MEDIATED ENHANCER DETECTION - A VERSATILE METHOD TO STUDY DEVELOPMENT IN *DROSOPHILA*. *Genes & Development*, **3**, 1288-1300.
- Ben-Ari, Y., Gaiarsa, J.L., Tyzio, R. & Khazipov, R. (2007) GABA: A pioneer transmitter that excites immature neurons and generates primitive oscillations. *Physiological Reviews*, **87**, 1215-1284.
- Bernhardt, R. & Matus, A. (1984) LIGHT AND ELECTRON-MICROSCOPIC STUDIES OF THE DISTRIBUTION OF MICROTUBULE-ASSOCIATED PROTEIN-2 IN RAT-BRAIN - A DIFFERENCE BETWEEN DENDRITIC AND AXONAL CYTOSKELETONS. *Journal of Comparative Neurology*, **226**, 203-221.
- Berman, R.F., Murray, K.D., Arque, G., Hunsaker, M.R., Wenzel, H.J. (2012) ABNORMAL DENDRITE AND SPINE MORPHOLOGY IN PRIMARY VISUAL CORTEX IN THE CGG KNOCK-IN MOUSE MODEL OF THE FRAGILE X PREMUTATION. *Epilepsia*, **53**, Suppl 1:150-60

- Boerner, J. & Duch, C. (2010) Average Shape Standard Atlas for the Adult *Drosophila* Ventral Nerve Cord. *Journal of Comparative Neurology*, **518**, 2437-2455.
- Borner, J., Puschmann, T. & Duch, C. (2006) A steroid hormone affects sodium channel expression in *Manduca* central neurons. *Cell and Tissue Research*, **325**, 175-187.
- Bouilleret, V., Schwaller, B., Schurmans, S., Celio, M.R. & Fritschy, J.M. (2000) Neurodegenerative and morphogenic changes in a mouse model of temporal lobe epilepsy do not depend on the expression of the calcium-binding proteins parvalbumin, calbindin, or calretinin. *Neuroscience*, **97**, 47-58.
- Brainbridge, S.P., Bownes, M. (1981) Staging the metamorphosis of *Drosophila melanogaster*. *Embryol. exp. Morph.*, **66**, pp. 57-80.
- Brand, A.H. & Perrimon, N. (1993) TARGETED GENE-EXPRESSION AS A MEANS OF ALTERING CELL FATES AND GENERATING DOMINANT PHENOTYPES. *Development*, **118**, 401-415.
- Briggman, K.L. & Denk, W. (2006) Towards neural circuit reconstruction with volume electron microscopy techniques. *Current Opinion in Neurobiology*, **16**, 562-570.
- Bullock, T.H., Bennett, M.V.L., Johnston, D., Josephson, R., Marder, E. & Fields, R.D. (2005) The Neuron Doctrine, redux. *Science*, **310**, 791-793.
- Burrows M. 1996. The neurobiology of an insect brain. Oxford: Oxford University Press. 682 p.
- Chang, K.T. & Berg, D.K. (2001) Voltage-gated channels block nicotinic regulation of CREB phosphorylation and gene expression in neurons. *Neuron*, **32**, 855-865.
- Clark, I.E., Jan, L.Y. & Jan, Y.N. (1997) Reciprocal localization of Nod and kinesin fusion proteins indicates microtubule polarity in the *Drosophila* oocyte, epithelium, neuron and muscle. *Development*, **124**, 461-470.
- Cline, H. (2005) Synaptogenesis: A balancing act between excitation and inhibition. *Current Biology*, **15**, R203-R205.
- Cline, H. & Haas, K. (2008) The regulation of dendritic arbor development and plasticity by glutamatergic synaptic input: a review of the synaptotrophic hypothesis. *Journal of Physiology-London*, **586**, 1509-1517.
- Cogshall, J.C. (1978) NEURONS ASSOCIATED WITH DORSAL LONGITUDINAL FLIGHT MUSCLES OF *DROSOPHILA-MELANOGASTER*. *Journal of Comparative Neurology*, **177**, 707-720.
- Connors, B.W. & Regehr, W.G. (1996) Neuronal firing: Does function follow form? *Current Biology*, **6**, 1560-1562.

- Consoulas, C., Duch, C., Bayline, R.J. & Levine, R.B. (2000) Behavioral transformations during metamorphosis: Remodeling of neural and motor systems. *Brain Research Bulletin*, **53**, 571-583.
- Consoulas, C., Restifo, L.L. & Levine, R.B. (2002) Dendritic remodeling and growth of motoneurons during metamorphosis of *Drosophila melanogaster*. *Journal of Neuroscience*, **22**, 4906-4917.
- Cooke, B.M. & Woolley, C.S. (2005) Gonadal hormone modulation of dendrites in the mammalian CNS. *Journal of Neurobiology*, **64**, 34-46.
- Cossart, R., Tyzio, R., Dinocourt, C., Esclapez, M., Hirsch, J.C., Ben-Ari, Y. & Bernard, C. (2001) Presynaptic kainate receptors that enhance the release of GABA on CA1 hippocampal interneurons. *Neuron*, **29**, 497-508.
- Cuntz, H., Borst, A. & Segev, I. (2007) Optimization principles of dendritic structure. *Theoretical Biology and Medical Modelling*, **4**, 8.
- Di Cristo, G., Wu, C.Z., Chattopadhyaya, B., Ango, F., Enott, G., Welker, E., Svoboda, K. & Huang, Z.J. (2004) Subcellular domain-restricted GABAergic innervation in primary visual cortex in the absence of sensory and thalamic inputs. *Nature Neuroscience*, **7**, 1184-1186.
- Dickinson, M.H. & Tu, M.S. (1997) The function of dipteran flight muscle. *Comparative Biochemistry and Physiology a-Physiology*, **116**, 223-238.
- Dinocourt, C., Petanjek, Z., Freund, T.F., Ben-Ari, Y. & Esclapez, M. (2003) Loss of interneurons innervating pyramidal cell dendrites and axon initial segments in the CA1 region of the hippocampus following pilocarpine-induced seizures. *Journal of Comparative Neurology*, **459**, 407-425.
- Duch, C. & Levine, R.B. (2000) Remodeling of membrane properties and dendritic architecture accompanies the postembryonic conversion of a slow into a fast motoneuron. *Journal of Neuroscience*, **20**, 6950-6961.
- Duch, C. & Mentel, T. (2004) Activity affects dendritic shape and synapse elimination during steroid controlled dendritic retraction in *Manduca sexta*. *Journal of Neuroscience*, **24**, 9826-9837.
- Duch, C., Vonhoff, F. & Ryglewski, S. (2008) Dendrite Elongation and Dendritic Branching Are Affected Separately by Different Forms of Intrinsic Motoneuron Excitability. *Journal of Neurophysiology*, **100**, 2525-2536.
- Duffy, J.B. (2002) GAL4 system in *Drosophila*: A fly geneticist's Swiss army knife. *Genesis*, **34**, 1-15.
- Duflocq, A., Chareyre, F., Giovannini, M., Couraud, F. & Davenne, M. (2011) Characterization of the axon initial segment (AIS) of motor neurons and identification of a para-AIS and a juxtapara-AIS, organized by protein 4.1B. *Bmc Biology*, **9**, 18.

- Enell, L., Hamasaka, Y., Kolodziejczyk, A. & Nassel, D.R. (2007) g-aminobutyric acid (GABA) signaling components in *Drosophila*: Immunocytochemical localization of GABA(B) receptors in relation to the GABA(A) receptor subunit RDL and a vesicular GABA transporter. *Journal of Comparative Neurology*, **505**, 18-31.
- Engel, J.E. & Wu, C.F. (1996) Altered habituation of an identified escape circuit in *Drosophila* memory mutants. *Journal of Neuroscience*, **16**, 3486-3499.
- Engel, J.E. & Wu, C.F. (1998) Genetic dissection of functional contributions of specific potassium channel subunits in habituation of an escape circuit in *Drosophila*. *Journal of Neuroscience*, **18**, 2254-2267.
- Esclapez, M., Hirsch, J.C., Khazipov, R., BenAri, Y. & Bernard, C. (1997) Operative GABAergic inhibition in hippocampal CA1 pyramidal neurons in experimental epilepsy. *Proceedings of the National Academy of Sciences of the United States of America*, **94**, 12151-12156.
- Evers, J.F., Schmitt, S., Sibila, M. & Duch, C. (2005) Progress in functional neuroanatomy: Precise automatic geometric reconstruction of neuronal morphology from confocal image stacks. *Journal of Neurophysiology*, **93**, 2331-2342.
- Ewing, A.W. (1979) NEUROMUSCULAR BASIS OF COURTSHIP SONG IN *DROSOPHILA* - ROLE OF THE DIRECT AND AXILLARY WING MUSCLES. *Journal of Comparative Physiology*, **130**, 87-93.
- Eybalin, M., Caicedo, A., Renard, N., Ruel, J. & Puel, J.L. (2004) Transient Ca<sup>2+</sup>-permeable AMPA receptors in postnatal rat primary auditory neurons. *European Journal of Neuroscience*, **20**, 2981-2989.
- Fayyazuddin, A., Zaheer, M.A., Hiesinger, P.R. & Bellen, H.J. (2006) The nicotinic acetylcholine receptor D alpha 7 is required for an escape behavior in *Drosophila*. *Plos Biology*, **4**, 420-431.
- Ffrenchconstant, R.H., Rocheleau, T.A., Steichen, J.C. & Chalmers, A.E. (1993) A POINT MUTATION IN A *DROSOPHILA* GABA RECEPTOR CONFERS INSECTICIDE RESISTANCE. *Nature*, **363**, 449-451.
- Ffrenchconstant, R.H., Roush, R.T., Mortlock, D. & Dively, G.P. (1990) ISOLATION OF DIELDRIN RESISTANCE FROM FIELD POPULATIONS OF *DROSOPHILA-MELANOGASTER* (DIPTERA, DROSOPHILIDAE). *Journal of Economic Entomology*, **83**, 1733-1737.
- Flavell, S.W. & Greenberg, M.E. (2008) Signaling mechanisms linking neuronal activity to gene expression and plasticity of the nervous system. *Annual Review of Neuroscience*, **31**, 563-590.
- French, A.S., Sanders, E.J., Duszyk, E., Prasad, S., Torkkeli, P.H., Haskins, J. & Murphy, R.A. (1993) IMMUNOCYTOCHEMICAL LOCALIZATION OF SODIUM-CHANNELS IN AN INSECT CENTRAL-NERVOUS-SYSTEM USING A SITE-DIRECTED ANTIBODY. *Journal of Neurobiology*, **24**, 939-948.

- Gao, F.B. & Bogert, B.A. (2003) Genetic control of dendritic morphogenesis in *Drosophila*. *Trends in Neurosciences*, **26**, 262-268.
- Gasparini, S. & Magee, J.C. (2006) State-dependent dendritic computation in hippocampal CA1 pyramidal neurons. *Journal of Neuroscience*, **26**, 2088-2100.
- Gordon, S. & Dickinson, M.H. (2006) Role of calcium in the regulation of mechanical power in insect flight. *Proceedings of the National Academy of Sciences of the United States of America*, **103**, 4311-4315.
- Grauso, M., Reenan, R.A., Culetto, E. & Sattelle, D.B. (2002) Novel putative nicotinic acetylcholine receptor subunit genes, D alpha 5, D alpha 6 and D alpha 7 in *Drosophila melanogaster* identify a new and highly conserved target of adenosine deaminase acting on RNA-mediated A-to-I pre-mRNA editing. *Genetics*, **160**, 1519-1533.
- Grueber, W.B., Jan, L.Y. & Jan, Y.N. (2003) Different levels of the homeodomain protein cut regulate distinct dendrite branching patterns of *Drosophila* multidendritic neurons. *Cell*, **112**, 805-818.
- Gulledge, A.T., Kampa, B.M. & Stuart, G.J. (2005) Synaptic integration in dendritic trees. *Journal of Neurobiology*, **64**, 75-90.
- Gulledge, A.T. & Stuart, G.J. (2003) Excitatory actions of GABA in the cortex. *Neuron*, **37**, 299-309.
- Guy, H.R. & Conti, F. (1990) PURSUING THE STRUCTURE AND FUNCTION OF VOLTAGE-GATED CHANNELS. *Trends in Neurosciences*, **13**, 201-206.
- Harcombe, E.S. & Wyman, R.J. (1977) OUTPUT PATTERN GENERATION BY DROSOPHILA FLIGHT MOTONEURONS. *Journal of Neurophysiology*, **40**, 1066-1077.
- Harcombe, E.S. & Wyman, R.J. (1978) CYCLICALLY REPETITIVE FIRING SEQUENCES OF IDENTIFIED DROSOPHILA FLIGHT MOTONEURONS. *Journal of Comparative Physiology*, **123**, 271-279.
- Harrison, J.B., Chen, H.H., Sattelle, E., Barker, P.J., Huskisson, N.S., Rauh, J.J., Bai, D. & Sattelle, D.B. (1996) Immunocytochemical mapping of a C-terminus anti-peptide antibody to the GABA receptor subunit, RDL in the nervous system of *Drosophila melanogaster*. *Cell and Tissue Research*, **284**, 269-278.
- Hartwig, C.L., Worrell, J., Levine, R.B., Ramaswami, M. & Sanyal, S. (2008) Normal dendrite growth in *Drosophila* motor neurons requires the AP-1 transcription factor. *Developmental Neurobiology*, **68**, 1225-1242.
- Hausser, M. & Mel, B. (2003) Dendrites: bug or feature? *Current Opinion in Neurobiology*, **13**, 372-383.
- Hausser, M., Spruston, N. & Stuart, G.J. (2000) Diversity and dynamics of dendritic signaling. *Science*, **290**, 739-744.

- Hedstrom, K.L., Xu, X.R., Ogawa, Y., Frischknecht, R., Seidenbecher, C.I., Shrager, P. & Rasband, M.N. (2007) Neurofascin assembles a specialized extracellular matrix at the axon initial segment. *Journal of Cell Biology*, **178**, 875-886.
- Hill, A.S., Nishino, A., Nakajo, K., Zhang, G.X., Fineman, J.R., Selzer, M.E., Okamura, Y. & Cooper, E.C. (2008) Ion Channel Clustering at the Axon Initial Segment and Node of Ranvier Evolved Sequentially in Early Chordates. *Plos Genetics*, **4**, 15.
- Hille, B. (1992) Ionic channels of excitable membranes, 2d ed. Sunderland, MA: Sinauer.
- Hines, M.L. & Carnevale, N.T. (1997) The NEURON simulation environment. *Neural Computation*, **9**, 1179-1209.
- Hohensee, S., Bleiss, W. & Duch, C. (2008) Correlative electron and confocal microscopy assessment of synapse localization in the central nervous system of an insect. *Journal of Neuroscience Methods*, **168**, 64-70.
- Horton, A.C. & Ehlers, M.D. (2003) Neuronal polarity and trafficking. *Neuron*, **40**, 277-295.
- Huang, E.J. & Reichardt, L.F. (2003) Trk receptors: Roles in neuronal signal transduction. *Annual Review of Biochemistry*, **72**, 609-642.
- Ikeda, K. & Koenig, J.H. (1988) MORPHOLOGICAL IDENTIFICATION OF THE MOTOR NEURONS INNERVATING THE DORSAL LONGITUDINAL FLIGHT-MUSCLE OF DROSOPHILA-MELANOGASTER. *Journal of Comparative Neurology*, **273**, 436-444.
- Jack, J.J.B., Noble, D., Tsien, R.W. Electric Current Flow in Excitable Cells. Oxford University Press, Oxford (1975), pp. 218-223
- Jan, L.Y. & Jan, Y.N. (1976) PROPERTIES OF LARVAL NEUROMUSCULAR-JUNCTION IN DROSOPHILA-MELANOGASTER. *Journal of Physiology-London*, **262**, 189-&.
- Jefferis, G., Marin, E.C., Stocker, R.F. & Luo, L.Q. (2001) Target neuron prespecification in the olfactory map of Drosophila. *Nature*, **414**, 204-208.
- Johnston, D., Magee, J.C., Colbert, C.M. & Christie, B.R. (1996) Active properties of neuronal dendrites. *Annual Review of Neuroscience*, **19**, 165-186.
- Kadas, D., Tzortzopoulos, A., Skoulakis, E.M.C. & Consoulas, C. (2012) Constitutive Activation of Ca<sup>2+</sup>/Calmodulin-Dependent Protein Kinase II during Development Impairs Central Cholinergic Transmission in a Circuit Underlying Escape Behavior in Drosophila. *Journal of Neuroscience*, **32**, 170-182.
- Kapfer, C., Seidl, A.H., Schweizer, H. & Grothe, B. (2002) Experience-dependent refinement of inhibitory inputs to auditory coincidence-detector neurons. *Nature Neuroscience*, **5**, 247-253.
- Katsuki, T., Ailani, D., Hiramoto, M. & Hiromi, Y. (2009) Intra-axonal Patterning: Intrinsic Compartmentalization of the Axonal Membrane in Drosophila Neurons. *Neuron*, **64**, 188-199.

- Katsuki, T., Joshi, R., Ailani, D. & Hiromi, Y. (2011) Compartmentalization Within Neurites: Its Mechanisms and Implications. *Developmental Neurobiology*, **71**, 458-473.
- Katz, L.C. & Shatz, C.J. (1996) Synaptic activity and the construction of cortical circuits. *Science*, **274**, 1133-1138.
- Katz, Y., Menon, V., Nicholson, D.A., Geinisman, Y., Kath, W.L. & Spruston, N. (2009) Synapse Distribution Suggests a Two-Stage Model of Dendritic Integration in CA1 Pyramidal Neurons. *Neuron*, **63**, 171-177.
- Kaufmann, W.E. & Moser, H.W. (2000) Dendritic anomalies in disorders associated with mental retardation. *Cerebral Cortex*, **10**, 981-991.
- Kim, S. & Chiba, A. (2004) Dendritic guidance. *Trends in Neurosciences*, **27**, 194-202.
- King, D.G. & Wyman, R.J. (1980) ANATOMY OF THE GIANT FIBER PATHWAY IN DROSOPHILA .1. 3 THORACIC COMPONENTS OF THE PATHWAY. *Journal of Neurocytology*, **9**, 753-770.
- Koch, C., Douglas, R. & Wehmeier, U. (1990) VISIBILITY OF SYNAPTICALLY INDUCED CONDUCTANCE CHANGES - THEORY AND SIMULATIONS OF ANATOMICALLY CHARACTERIZED CORTICAL PYRAMIDAL CELLS. *Journal of Neuroscience*, **10**, 1728-1744.
- Koch, C. & Segev, I. (2000) The role of single neurons in information processing. *Nature Neuroscience*, **3**, 1171-1177.
- Koenig, J.H. & Ikeda, K. (1980a) FLIGHT PATTERN INDUCED BY TEMPERATURE IN A SINGLE-GENE MUTANT OF DROSOPHILA-MELANOGASTER. *Journal of Neurobiology*, **11**, 509-517.
- Koenig, J.H. & Ikeda, K. (1980b) INTERSPIKE INTERVAL RELATIONSHIP AMONG FLIGHT-MUSCLE FIBERS IN DROSOPHILA. *Journal of Experimental Biology*, **87**, 137-147.
- Koenig, J.H. & Ikeda, K. (1980c) NEURAL INTERACTIONS CONTROLLING TIMING OF FLIGHT-MUSCLE ACTIVITY IN DROSOPHILA. *Journal of Experimental Biology*, **87**, 121-136.
- Kole, M.H.P., Ilschner, S.U., Kampa, B.M., Williams, S.R., Ruben, P.C. & Stuart, G.J. (2008) Action potential generation requires a high sodium channel density in the axon initial segment. *Nature Neuroscience*, **11**, 178-186.
- Kole, M.H.P. & Stuart, G.J. (2008) Is action potential threshold lowest in the axon? *Nature Neuroscience*, **11**, 1253-1255.
- Komiyama, T. & Luo, L. (2007) Intrinsic control of precise dendritic targeting by an ensemble of transcription factors. *Current Biology*, **17**, 278-285.
- Kulkarni, S.J., Newby, L.M. & Jackson, F.R. (1994) DROSOPHILA GABAERGIC SYSTEMS .2. MUTATIONAL ANALYSIS OF CHROMOSOMAL SEGMENT 64AB, A REGION CONTAINING THE GLUTAMIC-ACID DECARBOXYLASE GENE. *Molecular & General Genetics*, **243**, 555-564.

- Landgraf, M. & Thor, S. (2006) Development of *Drosophila* motoneurons: Specification and morphology. *Seminars in Cell & Developmental Biology*, **17**, 3-11.
- Lee, D., Su, H.L. & O'Dowd, D.K. (2003) GABA receptors containing Rdl subunits mediate fast inhibitory synaptic transmission in *Drosophila* neurons. *Journal of Neuroscience*, **23**, 4625-4634.
- Lee, S.B., Bagley, J.A., Lee, H.Y., Jan, L.Y. & Jan, Y.N. (2011) Pathogenic polyglutamine proteins cause dendrite defects associated with specific actin cytoskeletal alterations in *Drosophila*. *Proceedings of the National Academy of Sciences of the United States of America*, **108**, 16795-16800.
- Leech, C.A. & Sattelle, D.B. (1993) Acetylcholine receptor/channel molecules of insects. *EXS*, **63**, 81-97.
- Levine, J.D. & Wyman, R.J. (1973) NEUROPHYSIOLOGY OF FLIGHT IN WILD-TYPE AND A MUTANT *DROSOPHILA*. *Proceedings of the National Academy of Sciences of the United States of America*, **70**, 1050-1054.
- Liu, G.S. (2004) Local structural balance and functional interaction of excitatory and inhibitory synapses in hippocampal dendrites. *Nature Neuroscience*, **7**, 373-379.
- Liu, X., Krause, W.C. & Davis, R.L. (2007) GABA(A) receptor RDL inhibits *Drosophila* olfactory associative learning. *Neuron*, **56**, 1090-1102.
- London, M. & Hausser, M. (2005) Dendritic computation *Annual Review of Neuroscience*. Annual Reviews, Palo Alto, pp. 503-532.
- Lorincz, A. & Nusser, Z. (2010) Molecular Identity of Dendritic Voltage-Gated Sodium Channels. *Science*, **328**, 906-909.
- LoTurco, J.J., Owens, D.F., Heath, M.J.S., Davis, M.B.E. & Kriegstein, A.R. (1995) GABA and glutamate depolarize cortical progenitor cells and inhibit DNA synthesis. *Neuron*, **15**, 1287-1298.
- Loughney, K., Kreber, R., Ganetzky, B. (1989) Molecular analysis of the *DmNa V* locus, a sodium channel gene. *Drosophila*. *Cell*, **58**, 1143-1154.
- Luo, L.Q. (2000) Rho GTPases in neuronal morphogenesis. *Nature Reviews Neuroscience*, **1**, 173-180.
- Machin, K.E. & Pringle, J.W.S. (1959) THE PHYSIOLOGY OF INSECT FIBRILLAR MUSCLE .2. MECHANICAL PROPERTIES OF A BEETLE FLIGHT MUSCLE. *Proceedings of the Royal Society of London Series B-Biological Sciences*, **151**, 204-225.
- Magee, J.C. & Cook, E.P. (2000) Somatic EPSP amplitude is independent of synapse location in hippocampal pyramidal neurons. *Nature Neuroscience*, **3**, 895-903.
- Mainen, Z.F. & Sejnowski, T.J. (1996) Influence of dendritic structure on firing pattern in model neocortical neurons. *Nature*, **382**, 363-366.

- Markram, H., Helm, P.J. & Sakmann, B. (1995) DENDRITIC CALCIUM TRANSIENTS EVOKED BY SINGLE BACK-PROPAGATING ACTION-POTENTIALS IN RAT NEOCORTICAL PYRAMIDAL NEURONS. *Journal of Physiology-London*, **485**, 1-20.
- Megias, M., Emri, Z., Freund, T.F. & Gulyas, A.I. (2001) Total number and distribution of inhibitory and excitatory synapses on hippocampal CA1 pyramidal cells. *Neuroscience*, **102**, 527-540.
- Mehta, M.R. (2004) Cooperative LTP can map memory sequences on dendritic branches. *Trends in Neurosciences*, **27**, 69-72.
- Meseke, M., Evers, J.F. & Duch, C. (2009a) Developmental Changes in Dendritic Shape and Synapse Location Tune Single-Neuron Computations to Changing Behavioral Functions. *Journal of Neurophysiology*, **102**, 41-58.
- Meseke, M., Evers, J.F. & Duch, C. (2009b) PTX-induced hyperexcitability affects dendritic shape and GABAergic synapse density but not synapse distribution during *Manduca* postembryonic motoneuron development. *Journal of Comparative Physiology a-Neuroethology Sensory Neural and Behavioral Physiology*, **195**, 473-489.
- Migues, P.V., Cammarota, M., Kavanagh, J., Atkinson, R., Powis, D.A. & Rostas, J.A.P. (2007) Maturation changes in the subunit composition of AMPA receptors and the functional consequences of their activation in chicken forebrain. *Developmental Neuroscience*, **29**, 232-240.
- Miles, R. (1990) SYNAPTIC EXCITATION OF INHIBITORY CELLS BY SINGLE CA3 HIPPOCAMPAL PYRAMIDAL CELLS OF THE GUINEA-PIG INVITRO. *Journal of Physiology-London*, **428**, 61-77.
- Montague, P.R. & Friedlander, M.J. (1989) EXPRESSION OF AN INTRINSIC GROWTH STRATEGY BY MAMMALIAN RETINAL NEURONS. *Proceedings of the National Academy of Sciences of the United States of America*, **86**, 7223-7227.
- Montague, P.R. & Friedlander, M.J. (1991) MORPHOGENESIS AND TERRITORIAL COVERAGE BY ISOLATED MAMMALIAN RETINAL GANGLION-CELLS. *Journal of Neuroscience*, **11**, 1440-1457.
- Moore, A.W., Jan, L.Y. & Jan, Y.N. (2002) hamlet, a binary genetic switch between single- and multiple-dendrite neuron morphology. *Science*, **297**, 1355-1358.
- Nguyen, L., Rigo, J.M., Rocher, V., Belachew, S., Malgrange, B., Rogister, B., Leprince, P. & Moonen, G. (2001) Neurotransmitters as early signals for central nervous system development. *Cell and Tissue Research*, **305**, 187-202.
- Nicholson, D.A., Trana, R., Katz, Y., Kath, W.L., Spruston, N. & Geinisman, Y. (2006) Distance-dependent differences in synapse number and AMPA receptor expression in hippocampal CA1 pyramidal neurons. *Neuron*, **50**, 431-442.

- Oliveira, E.E., Pippow, A., Salgado, V.L., Buschges, A., Schmidt, J. & Kloppenburg, P. (2010) Cholinergic Currents in Leg Motoneurons of *Carausius morosus*. *Journal of Neurophysiology*, **103**, 2770-2782.
- Owens, D.F. & Kriegstein, A.R. (2002) Developmental neurotransmitters? *Neuron*, **36**, 989-991.
- Palmer, L.M. & Stuart, G.J. (2006) Site of action potential initiation in layer 5 pyramidal neurons. *Journal of Neuroscience*, **26**, 1854-1863.
- Pan, Z.M., Kao, T.C., Horvath, Z., Lemos, J., Sul, J.Y., Cranstoun, S.D., Bennett, V., Scherer, S.S. & Cooper, E.C. (2006) A common ankyrin-G-based mechanism retains KCNQ and Na-V channels at electrically active domains of the axon. *Journal of Neuroscience*, **26**, 2599-2613.
- Polleux, F., Morrow, T. & Ghosh, A. (2000) Semaphorin 3A is a chemoattractant for cortical apical dendrites. *Nature*, **404**, 567-573.
- Pouille, F. & Scanziani, M. (2001) Enforcement of temporal fidelity in pyramidal cells by somatic feed-forward inhibition. *Science*, **293**, 1159-1163.
- Raghu, S.V., Joesch, M., Borst, A. & Reiff, D.F. (2007) Synaptic organization of lobula plate tangential cells in *Drosophila*: gamma-aminobutyric acid receptors and chemical release sites. *Journal of Comparative Neurology*, **502**, 598-610.
- Raghu, S.V., Joesch, M., Sigrist, S.J., Borst, A. & Reiff, D.F. (2009) Synaptic Organization of Lobula Plate Tangential Cells in *Drosophila*: D7 Cholinergic Receptors. *Journal of Neurogenetics*, **23**, 200-209.
- Rall W. (1962a) Theory of physiological properties of dendrites. *Ann. N.Y. Acad. Sci.* **96**: 1071-1092.
- Rall W. (1962b) Electrophysiology of a dendritic neuron model. *Biophys. J.* **2**:145-167.
- Rall W. (1964) Theoretical significance of dendritic trees for neuronal input-output relations. In *Neural Theory and Modeling*, ed. R.F. Reiss. Stanford Univ. Press.
- Rall, W. (1967) DISTINGUISHING THEORETICAL SYNAPTIC POTENTIALS COMPUTED FOR DIFFERENT SOMA-DENDRITIC DISTRIBUTIONS OF SYNAPTIC INPUT. *Journal of Neurophysiology*, **30**, 1138-&.
- Ramon-Moliner E. 1968. The morphology of dendrites. In *the Structure And Function of Nervous Tissue*, ed. GH Bourne, pp. 205-67. New York Academic
- Ramon y Cajal (1897) Las leyes de la morfología y dinamismo de las células nerviosas. *Revista Trim Microgr* 1.
- Rasband, M.N. (2010) The axon initial segment and the maintenance of neuronal polarity. *Nature Reviews Neuroscience*, **11**, 552-562.

- Redman, S. & Walmsley, B. (1983) THE TIME COURSE OF SYNAPTIC POTENTIALS-EVOKED IN CAT SPINAL MOTONEURONES AT IDENTIFIED GROUP-IA SYNAPSES. *Journal of Physiology-London*, **343**, 117-&.
- Redmond, L. & Ghosh, A. (2005) Regulation of dendritic development by calcium signaling. *Cell Calcium*, **37**, 411-416.
- Rinzel, J. & Rall, W. (1974) TRANSIENT-RESPONSE IN A DENDRITIC NEURON MODEL FOR CURRENT INJECTED AT ONE BRANCH. *Biophysical Journal*, **14**, 759-790.
- Rolls, M.M., Satoh, D., Clyne, P.J., Henner, A.L., Uemura, T. & Doe, C.Q. (2007) Polarity and intracellular compartmentalization of Drosophila neurons. *Neural Development*, **2**.
- Ryglewski, S. & Duch, C. (2009) Shaker and Shal Mediate Transient Calcium-Independent Potassium Current in a Drosophila Flight Motoneuron. *Journal of Neurophysiology*, **102**, 3673-3688.
- Ryglewski, S., Lance, K., Levine, R.B. & Duch, C. (2012) Ca(v)2 channels mediate low and high voltage-activated calcium currents in Drosophila motoneurons. *Journal of Physiology-London*, **590**, 809-825.
- Ryglewski, S., Pflueger, H.J. & Duch, C. (2007) Expanding the neuron's calcium signaling repertoire: Intracellular calcium release via voltage-induced PLC and IP3R activation. *Plos Biology*, **5**, 818-827.
- Sanchez-Soriano, N., Bottenberg, W., Fiala, A., Haessler, U., Kerassoviti, A., Knust, E., Lohr, R. & Prokop, A. (2005) Are dendrites in Drosophila homologous to vertebrate dendrites? *Developmental Biology*, **288**, 126-138.
- Sanyal, S. (2009) Genomic mapping and expression patterns of C380, OK6 and D42 enhancer trap lines in the larval nervous system of Drosophila. *Gene Expression Patterns*, **9**, 371-380.
- Sanyal, S., Narayanan, R., Consoulas, C. & Ramaswami, M. (2003) Evidence for cell autonomous AP1 function in regulation of Drosophila motor-neuron plasticity. *Bmc Neuroscience*, **4**.
- Schmitt, S., Evers, J.F., Duch, C., Scholz, M. & Obermayer, K. (2004) New methods for the computer-assisted 3-D reconstruction of neurons from confocal image stacks. *Neuroimage*, **23**, 1283-1298.
- Somogyi, P., Tamas, G., Lujan, R. & Buhl, E.H. (1998) Salient features of synaptic organisation in the cerebral cortex. *Brain Research Reviews*, **26**, 113-135.
- Spatkowski, G. & Schilling, K. (2003) Postnatal dendritic morphogenesis of cerebellar basket and stellate cells in vitro. *Journal of Neuroscience Research*, **72**, 317-326.
- Staley, K.J. & Mody, I. (1992) SHUNTING OF EXCITATORY INPUT TO DENTATE GYRUS GRANULE CELLS BY A DEPOLARIZING GABA-A RECEPTOR-MEDIATED POSTSYNAPTIC CONDUCTANCE. *Journal of Neurophysiology*, **68**, 197-212.

- Stief, F., Zuschratter, W., Hartmann, K., Schmitz, D. & Draguhn, A. (2007) Enhanced synaptic excitation-inhibition ratio in hippocampal interneurons of rats with temporal lobe epilepsy. *European Journal of Neuroscience*, **25**, 519-528.
- Stilwell, G.E., Rocheleau, T. & Frenchconstant, R.H. (1995) GABA RECEPTOR MINIGENE RESCUES INSECTICIDE RESISTANCE PHENOTYPES IN DROSOPHILA. *Journal of Molecular Biology*, **253**, 223-227.
- Stuart, G.J. & Hausser, M. (2001) Dendritic coincidence detection of EPSDs and action potentials. *Nature Neuroscience*, **4**, 63-71.
- Tamas, G., Szabadics, J. & Somogyi, P. (2002) Cell type- and subcellular position-dependent summation of unitary postsynaptic potentials in neocortical neurons. *Journal of Neuroscience*, **22**, 740-747.
- Thackeray, J.R. & Ganetzky, B. (1994) DEVELOPMENTALLY-REGULATED ALTERNATIVE SPLICING GENERATES A COMPLEX ARRAY OF DROSOPHILA-PARA SODIUM-CHANNEL ISOFORMS. *Journal of Neuroscience*, **14**, 2569-2578.
- Tripodi, M., Evers, J.F., Mauss, A., Bate, M. & Landgraf, M. (2008) Structural Homeostasis: Compensatory Adjustments of Dendritic Arbor Geometry in Response to Variations of Synaptic Input. *Plos Biology*, **6**, 2172-2187.
- Trunova, S., Baek, B. & Giniger, E. (2011) Cdk5 Regulates the Size of an Axon Initial Segment-Like Compartment in Mushroom Body Neurons of the Drosophila Central Brain. *Journal of Neuroscience*, **31**, 10451-10462.
- Urban, N.N. & Castro, J.B. (2010) Functional polarity in neurons: what can we learn from studying an exception? *Current Opinion in Neurobiology*, **20**, 538-542.
- van Vliet, E.A., Aronica, E., Tolner, E.A., da Silva, F.H.L. & Gorter, J.A. (2004) Progression of temporal lobe epilepsy in the rat is associated with immunocytochemical changes in inhibitory interneurons in specific regions of the hippocampal formation. *Experimental Neurology*, **187**, 367-379.
- Van Wart, A., Trimmer, J.S. & Matthews, G. (2007) Polarized distribution of ion channels within microdomains of the axon initial segment. *Journal of Comparative Neurology*, **500**, 339-352.
- Vetter, P., Roth, A. & Hausser, M. (2001) Propagation of action potentials in dendrites depends on dendritic morphology. *Journal of Neurophysiology*, **85**, 926-937.
- Vonhoff, F. & Duch, C. (2010) Tiling Among Stereotyped Dendritic Branches in an Identified Drosophila Motoneuron. *Journal of Comparative Neurology*, **518**, 2169-2185.
- Weeks, J.C. & Levine, R.B. (1995) Steroid hormone effects on neurons subserving behavior. *Current Opinion in Neurobiology*, **5**, 809-815.
- West, A.E., Griffith, E.C. & Greenberg, M.E. (2002) Regulation of transcription factors by neuronal activity. *Nature Reviews Neuroscience*, **3**, 921-931.

- Wong, R.O.L. & Ghosh, A. (2002) Activity-dependent regulation of dendritic growth and patterning. *Nature Reviews Neuroscience*, **3**, 803-812.
- Zhou, D.X., Lambert, S., Malen, P.L., Carpenter, S., Boland, L.M. & Bennett, V. (1998) Ankyring is required for clustering of voltage-gated Na channels at axon initial segments and for normal action potential firing. *Molecular Biology of the Cell*, **9**, 37A-37A.